During heat stress in *Myxococcus xanthus*, the CdbS PilZ domain protein, along with two PilZ-DnaK chaperones, perturbs chromosome organization and accelerates cell death

Michael Seidel[1], Dorota Skotnicka[1], Timo Glatter[2] and Lotte Søgaard-Andersen[1, 3]

[1] Department of Ecophysiology, Max Planck Institute for Terrestrial Microbiology, 35043 Marburg, Germany

[2] Core Facility for Mass Spectrometry & Proteomics, Max Planck Institute for Terrestrial Microbiology, 35043 Marburg, Germany

[3] Corresponding author

Tel. +49-(0)6421-178201

Fax +49-(0)6421-178209

E-mail: sogaard@mpi-marburg.mpg.de

Short title: The PilZ domain protein CdbS and regulated cell death.

Abstract

C-di-GMP is a bacterial second messenger that regulates diverse processes in response to environmental or cellular cues. The nucleoid-associated protein (NAP) CdbA in *Myxococcus xanthus* binds c-di-GMP and DNA in a mutually exclusive manner *in vitro*. CdbA is essential for viability, and CdbA depletion causes defects in chromosome organization, leading to a block in cell division and, ultimately, cell death. Most NAPs are not essential; therefore, to explore the paradoxical *cdbA* essentiality, we isolated suppressor mutations that restored cell viability without CdbA. Most mutations mapped to *cdbS*, which encodes a stand-alone c-di-GMP binding PilZ domain protein, and caused loss-of-function of *cdbS*. Cells lacking CdbA and CdbS or only CdbS were fully viable and had no defects in chromosome organization. CdbA depletion caused post-transcriptional upregulation of CdbS accumulation, and this CdbS over-accumulation was sufficient to disrupt chromosome organization and cause cell death. CdbA depletion also caused increased accumulation of CsdK1 and CsdK2, two unusual PilZ-DnaK chaperones. During CdbA depletion, CsdK1 and CsdK2, in turn, stabilized CdbS, thereby enabling its increased accumulation and toxicity. Moreover, we demonstrate that heat stress, possibly involving an increased cellular c-di-GMP concentration, induces the CdbA/CsdK1/CsdK2/CdbA system, causing a CsdK1- and CsdK2-dependent increase in CdbS accumulation. Thereby this system accelerates heat stress-induced chromosome mis-organization and cell death. Collectively, this work describes a unique system that contributes to regulated cell death in *M. xanthus* and suggests a link between c-di-GMP signaling and regulated cell death in bacteria.

Author summary

The nucleotide-based second messenger c-di-GMP in bacteria controls numerous processes in response to environmental or cellular cues. Typically, these processes are related to lifestyle transitions between motile and sessile behaviors. However, c-di-GMP also regulates other processes. In *Myxococcus xanthus*, CdbA is a DNA-binding and nucleoid-associated protein that helps to organize the large chromosome. CdbA binds c-di-GMP and DNA in a mutually exclusive manner. While other nucleoid-associated proteins are not essential, CdbA is essential. Here, we show that the crucial function of CdbA is to maintain the level of the c-di-GMP-binding PilZ-domain protein CdbS appropriately low. The CdbS level is not only increased upon depletion of CdbA but also in response to heat stress. Under both conditions, the increased CdbS level perturbs chromosome organization and ultimately causes cell death. The CdbA/CdbS system represents a unique system that contributes to

regulated cell death in *M. xanthus* and suggests a link between c-di-GMP signaling and regulated cell death.

Introduction

Bis-(3'-5')-cyclic dimeric GMP (c-di-GMP) is a versatile, ubiquitous nucleotide-based second messenger in bacteria involved in regulating diverse processes in response to environmental or cellular cues [1, 2]. The balance between the opposing activities of c-di-GMP synthesizing diguanylate cyclases and c-di-GMP-degrading phosphodiesterases determines the cellular c-di-GMP level [1, 2]. In addition to their enzymatically active domain, these enzymes often contain sensory domains that enable their regulation in response to specific cues [1, 2]. c-di-GMP binds to and allosterically regulates effectors to implement downstream responses at the transcriptional, translational or post-translational level [1, 2]. While DGCs and PDEs contain conserved domains, c-di-GMP-binding effector proteins are highly diverse and include, e.g. PilZ-domain proteins [3-7] and members of diverse transcription factor families as well as a nucleoid-associated protein [8-14]. C-di-GMP regulates many diverse processes, including biofilm formation, motility, adhesion, synthesis of secreted polysaccharides, cell cycle progression, development and virulence [1, 2]. Thereby, c-di-GMP contributes to fitness but is not essential. We recently reported an unexpected link between c-di-GMP and chromosome organization in *Myxococcus xanthus* mediated by CdbA, a c-di-GMP binding and nucleoid-associated protein (NAP) [11]. Typically, NAPs are small, abundant proteins that bind DNA with moderate sequence specificity causing bending, wrapping or bridging of DNA, thereby contributing to chromosome organization [15-17]. Generally, NAPs have minor effects on transcription and are not essential [15-17]; however, CdbA is essential [11]. Here, we focused on understanding the mechanism underlying CdbA essentiality.

M. xanthus is a Gram-negative bacterium with a nutrient-regulated biphasic lifecycle [18, 19]. Under nutrient-replete conditions, the rod-shaped cells proliferate and, using gliding motility and type IV pili (T4P)-dependent motility, generate coordinately spreading colonies in which cells also prey on other microbes. In response to nutrient depletion, a developmental program initiates that culminates in the formation of multicellular, spore-filled fruiting bodies. C-di-GMP accumulates during growth and at a ~10-fold higher level during development [20, 21]. During growth, c-di-GMP regulates T4P-dependent motility and the composition of the extracellular matrix including synthesis of the secreted polysaccharide exopolysaccharide [20, 22, 23]. During development, the increased c-di-GMP level is essential for fruiting body

formation and sporulation [21, 24]. Several c-di-GMP binding effectors involved in implementing these responses have been characterized [21-23]. The rod-shaped *M. xanthus* cells divide at midcell between two fully segregated chromosomes [25, 26]. Each daughter cell contains a single, fully replicated chromosome with the *ori* and *ter* regions anchored in the subpolar regions close to the old and new cell pole, respectively by a scaffold composed of the BacNOP bactofilins and the PadC adaptor [27-30]. Chromosome replication is initiated once per cell cycle and soon after cell division [29]. Segregation occurs parallel with replication and depends on a classical ParAB*S* system, in which ParB binds to centromere-like *parS* sites close to the *ori* while the ParA ATPase mediates segregation [29-31]. Segregation also depends on the structural maintenance of chromosome (SMC) complex, which contributes to separating the two daughter chromosomes [32, 33]. During segregation, one ParB/*parS* nucleoprotein complex remains in the subpolar region of the old pole while the second copy translocates to the subpolar region of the opposite pole [29].

CdbA and its paralog CdbB belong to the widespread ribbon-helix-helix superfamily of DNA binding protein, and all fully sequenced Myxococcales genomes encode at least one ortholog [11, 34]. While CdbA is essential for viability, CdbB is not [11]. CdbA depletion results in disrupted chromosome organization and impeded chromosome segregation, causing cell division defects, cellular filamentation, and eventually, cell lysis and death [11]. CdbA and CdbB bind c-di-GMP *in vitro* [11]. The binding of c-di-GMP does not alter the tetrameric state of CdbA but its conformation [11]. Importantly, DNA and c-di-GMP binding by CdbA involve the same interface of the tetramer and is mutually exclusive *in vitro* [11]. Consistently, CdbA variants that cannot bind c-di-GMP do not bind DNA *in vitro* and are non-functional *in vivo* [11]. In ChIP-seq analyses, CdbA binds >550 sites in the *M. xanthus* genome with moderate sequence specificity [11]. However, CdbA depletion causes no or only minor changes in transcription [11]. Based on these observations, and because CdbA is highly abundant with an average cell containing ~7000 CdbA monomers, we suggested that CdbA is an essential, ligand-regulated NAP and that c-di-GMP modulates DNA binding by CdbA [11]. According to this model, the primary function of CdbA is in chromosome organization, thereby supporting chromosome segregation, and the inhibition of cell division is a secondary effect caused by the defects in chromosome organization and segregation [11].

To investigate the mechanism underlying CdbA essentiality, we isolated suppressor mutations that restored cell viability without CdbA. Most mutations mapped to a gene that encodes a c-di-GMP-binding PilZ domain protein, which we named CdbS, and caused loss-of-function of *cdbS*. Cells lacking CdbA and CdbS or only CdbS were fully viable and had no evident defects in chromosome organization. CdbA depletion increased CdbS accumulation

dependent on two unusual PilZ-DnaK chaperones, which we named CsdK1 and CsdK2. Furthermore, an increased CdbS accumulation was sufficient to disrupt chromosome organization and, ultimately, cause cell death. We identify heat stress as a physiological cue causing increased CdbS accumulation in a CsdK1 and CsdK2-dependent manner, thereby contributing to chromosome mis-organization and cell death in response to heat stress.

Results

Isolation of suppressor mutants that are viable in the absence of CdbA

To investigate how the lack of CdbA is toxic to cells, we sought spontaneous suppressor mutants that were viable without CdbA. To this end, we used a strain with an in-frame deletion of native *cdbA* (Δ*cdbA*) in which ectopic expression of an active *cdbA-mCherry* (from here on CdbA-mCh) fusion is controlled by a vanillate-inducible promoter (P_{van}) [11]. Even when P_{van} is maximally induced in this strain in the presence of 500μM vanillate, the cellular level of CdbA-mCh is lower than when *cdbA-mCherry* is expressed from the native site and, therefore, this strain has a lower growth rate than the *cdbA*$^+$ WT strain [11]. Upon removal of vanillate, and correlating with the earliest time-point at ~24hrs at which CdbA-mCh is no longer detectable by immunoblotting, growth of this strain arrests and cells eventually lyse [11]. After plating cells on CTT broth without vanillate, 20 independent mutants were isolated that grew in the absence of vanillate. Sequence analysis demonstrated that six mutants had mutations in the vanillate-inducible promoter or in the gene encoding the vanillate repressor. By immunoblot analysis, six of the remaining 14 strains accumulated CdbA-mCh without vanillate. The remaining eight strains did not accumulate CdbA-mCh in the absence of vanillate and, thus, were viable in the absence of CdbA-mCh. Whole genome sequencing revealed that one suppressor strain had a mutation in *cdbB*, which encodes the paralog of CdbA, resulting in a Q22R substitution in CdbB (Table S1). The seven remaining suppressor strains had four different mutations in *mxan_4328* (Fig 1A; Table S1). *Mxan_4328* encodes a stand-alone PilZ domain protein (Fig 1AB) [23] and is not part of an operon [24] (S1A Fig). From here on, we focus on *mxan_4328*, which we named *cdbS* (CdbA essentiality suppressor).

The PilZ-domain protein CdbS binds c-di-GMP

The CdbS PilZ domain contains the conserved bipartite c-di-GMP binding motif characteristic of PilZ domains [2] (Fig 1B). A high-confidence AlphaFold-based structural model predicts monomeric CdbS as a six-stranded β-barrel typical of PilZ domains, but the

α-helix at the C-terminus characteristic of canonical PilZ domains was not predicted (Fig 1C; S2A Fig), classifying CdbS as an xPilZ domain protein [35]. CdbS is conserved in the *Cystobacterineae* and *Nannocystineae* suborders but not in the *Sorangineae* suborder of the Myxococcales [23] (S1BC Fig). The genetic neighbourhood of *cdbS* is conserved but encodes neither proteins with a predicted function in chromosome organization and segregation nor in cell division (S1C Fig). A systematic analysis of PilZ domain proteins in *M. xanthus* previously demonstrated that CdbS is dispensable for viability, motility, exopolysaccharide synthesis, and development [23].

We tested whether CdbS binds c-di-GMP using purified His_6-CdbS and His_6-$CdbS^{R9A}$, which contains the Arg9Ala substitution in the c-di-GMP binding motif and abolishes c-di-GMP binding by the PilZ domain protein YcgR [6] (Fig 1B; S2B Fig). Using bio-layer interferometry with a streptavidin sensor on which biotinylated c-di-GMP was immobilized, titration experiments revealed that His_6-CdbS binds c-di-GMP with a K_d of ~1.4μM, while His_6-$CdbS^{R9A}$ did not detectably bind c-di-GMP (Fig 1DE). This K_d is similar to that of other c-di-GMP binding PilZ domains [3, 5, 6]. The estimated cellular concentration of c-di-GMP in *M. xanthus* is ~1.4μM [11, 20], suggesting that CdbS binds c-di-GMP *in vivo*.

Essentiality of CdbA depends on CdbS

Two of the *cdbS* suppressor mutations map upstream of the *cdbS* transcription start site, one results in a premature stop codon at Gln76, and one in a Val32Gly substitution (Fig 1A; S1C Fig; S1 Table). We, therefore, hypothesized that the suppressor mutations cause loss-of-function of *cdbS*. To test this idea, we generated an in-frame deletion in *cdbS* (Δ*cdbS*) in the Δ*cdbA* strain in which *cdbA-mCh* is expressed from P_{van}. To follow chromosome organization, all strains ectopically expressed a *parB-YFP* fusion from the native promoter integrated in a single copy at the MxB *attB* site, generating merodiploid *parB*$^+$/*attB*::P_{nat}*parB-YFP* strains.

As reported [11], the CdbA-mCh depletion strain grew when supplemented with vanillate and at a lower rate than WT, and removal of vanillate caused (1) growth arrest after ~24hrs followed by a decrease in the optical density at 550nm (OD_{550}) indicating cell lysis, and (2) a three-log defect in plating efficiency (Fig 2A). Importantly, cells with the Δ*cdbS* mutation in the CdbA-mCh depletion strain were viable in the absence of vanillate and had a growth rate similar to WT (Fig 2A). Moreover, when a *cdbS-FLAG* allele was expressed ectopically under the control of the native promoter (P_{nat}) from a single copy integrated at the Mx8 *attB* site in the Δ*cdbS* CdbA-mCh depletion strain, this strain phenocopied the *cdbS*$^+$ CdbA-mCh depletion strain and had a growth defect in the absence of vanillate (Fig 2A). Thus, CdbS-FLAG is active and complements the Δ*cdbS* mutation. Finally, the Δ*cdbS* mutation in the

206 presence of CdbA did not affect viability and growth in agreement with previous findings [23]
207 (Fig 2A). Thus, the toxicity caused by lack of CdbA is suppressed by the lack of CdbS. In
208 other words, the essentiality of CdbA depends on the presence of CdbS, while the lack of
209 CdbS by itself affects neither growth nor viability.

210 As reported [11], the CdbA-mCh depletion strain supplemented with vanillate had a slightly
211 increased cell length compared to WT, while cells depleted of CdbA-mCh for 24hrs were
212 filamentous (Fig 2B). Importantly, Δ*cdbS* cells depleted of CdbA-mCh had a cell length
213 similar to WT. Moreover, cells were filamentous without vanillate upon ectopic expression of
214 active *cdbS-FLAG* in this strain. Finally, the Δ*cdbS* mutation in the presence of CdbA did not
215 affect cell length.

216 To assess chromosome organization, cells were stained with 4′,6-diamidino-2-phenylindole
217 (DAPI). As reported [25], short WT cells had one nucleoid centered around midcell, while
218 longer cells had two well-separated nucleoids centered around the quarter cell length
219 positions (Fig 2B). Furthermore, the ParB-YFP cluster(s) localized in the subpolar region(s)
220 and close to the outer edges of the nucleoid(s) (Fig 2B). The same pattern was observed for
221 the CdbA-mCh depletion strain in the presence of vanillate. However, and as reported [11],
222 after 24hrs in the absence of vanillate, and thus depleted of CdbA-mCh, cells had an
223 irregular distribution of the nucleoids and ParB-YFP clusters along the cell length (Fig 2B).
224 Strikingly, Δ*cdbS* cells depleted of CdbA-mCh had nucleoids and ParB-YFP clusters
225 organized as in WT (Fig 2B). Moreover, ectopic expression of CdbS-FLAG in these cells
226 resulted in an irregular distribution of the nucleoids and ParB-YFP clusters along the cell
227 length (Fig 2B). Finally, cells lacking only CdbS, had nucleoids and ParB-YFP clusters
228 organized as in WT, as expected from the lack of a growth defect (Fig 2B).

229 We conclude that lack of CdbA *per se* does not result in disrupted chromosome organization
230 with subsequent cellular filamentation and cell death. Instead, these defects are only
231 observed when CdbA is depleted in the presence of CdbS. Thus, CdbS is the critical factor
232 during CdbA depletion that mediates the disrupted chromosome organization, resulting in
233 cellular filamentation and cell death. Equally, the observation that lack of CdbS in otherwise
234 WT affects neither the chromosome nor viability demonstrates that CdbS is not essential for
235 these two processes. These observations support a model in which a lack of CdbA
236 unleashes CdbS activity.

237

238 Overexpression of *cdbS* phenocopies CdbA-depletion

239 To understand the connection between CdbA and CdbS, we asked whether CdbA regulates
240 *cdbS* expression. In published data [11], CdbA has a ChIP-seq peak centered at position -71

241 relative to the *cdbS* transcription start site at +1 (Fig 1A). Nevertheless, in RT-qPCR
242 analyses, the *cdbS* transcript level in the CdbA-mCh depletion strain in the presence and
243 absence of CdbA-mCh was not significantly different (Fig 3A).

244 To determine whether CdbA regulates CdbS accumulation post-transcriptionally, we
245 generated strains synthesizing CdbS-FLAG from the native site. In the CdbA-mCh depletion
246 strain in the presence of vanillate, CdbS-FLAG accumulated at a level similar to that of a
247 *cdbA*$^{+}$ strain in immunoblots with α-FLAG antibodies. But upon depletion of CdbA-mCh, the
248 CdbS-FLAG level increased ~4-fold (Fig 3B). Because *cdbS* transcription is not increased
249 upon CdbA-mCh depletion, we conclude that the increased CdbS level is the result of either
250 increased *cdbS* translation or increased CdbS stability.

251 To examine whether an increased CdbS level is sufficient to disrupt chromosome
252 organization and cause cell death, we ectopically expressed *cdbS-FLAG* under the control of
253 P_{van} in a Δ*cdbS* strain. In the absence of vanillate, CdbS-FLAG was not detectable in
254 immunoblots with α-FLAG antibodies (Fig 3C), cells had a growth rate, a mean cell length,
255 and the nucleoid as well as ParB-YFP clusters organized as in WT (Fig 3DE). In the
256 presence of vanillate for 24hrs, CdbS-FLAG accumulation was ~4-fold increased relative to
257 the strain expressing *cdbS-FLAG* from the native site (Fig 3C). Notably, at ~24hrs growth
258 was arrested followed by a decrease in OD_{550} indicating cell death, cells were filamentous,
259 and the nucleoid as well as ParB-YFP cluster localization were highly disorganized (Fig
260 3DE). Increasing or decreasing the cellular CdbS-FLAG level changed neither the cellular
261 level of CdbA-mCh nor its localization over the nucleoid (Fig 3FG). Moreover, ~4-fold
262 overexpression of the non-c-di-GMP binding CdbS^{R9A}-FLAG variant phenocopied cells
263 overexpressing CdbS-FLAG (S3AB Fig). Thus, cells overexpressing CdbS-FLAG ~4-fold
264 phenocopy cells depleted of CdbA-mCh and, under these conditions, the effect of CdbS-
265 FLAG overexpression is independent of c-di-GMP binding.

266 In control experiments, we treated WT with cephalexin to specifically inhibit cell division but
267 not chromosome organization [25]. After for 8hrs, cells had elongated and had two to four
268 well-separated nucleoids arranged regularly along the cell length, as well as an increased
269 number of ParB-YFP clusters, arranged evenly along the outer edges of the nucleoids (Fig
270 3E). These observations support that the primary defect in cells overexpressing CdbS-
271 FLAG, similar to cells depleted of CdbA-mCh, is in chromosome organization, not cell
272 division.

273 Altogether, we conclude that an elevated CdbS level is sufficient to disrupt chromosome
274 organization, thereby causing cellular filamentation and cell death. Because this phenotype
275 mirrors the phenotype caused by CdbA depletion, these observations suggest a genetic

pathway in which CdbA inhibits the accumulation of CdbS (Fig 3H). CdbA depletion alleviates this inhibition, and CdbS accumulates at an increased level. The increased CdbS level, in turn, interferes with chromosome organization, thereby inhibiting cell division and causing cellular filamentation and, eventually, cell death.

CdbS pulls down the DnaB helicase, chaperones and co-chaperones

To understand how CdbA depletion results in increased CdbS accumulation and how this over-accumulation may result in disrupted chromosome organization, we searched for protein interaction partners of CdbA and CdbS using pull-down experiments. An active CdbA-FLAG protein expressed from the native site significantly enriched CdbB and a putative lipoprotein but not CdbS (Fig 4A). This observation agrees with bacterial adenylate cyclase-based two-hybrid (BACTH) analyses demonstrating that CdbA and CdbB interact [11]. Because CdbA is a cytoplasmic protein and the putative lipoprotein is periplasmic, we did not consider this protein further. The active CdbS-FLAG expressed from the native site pulled-down 11 significantly enriched proteins (Fig 4B). These proteins did not include CdbA. These observations support that CdbA and CdbS do not interact directly and that the effect of CdbA-depletion on CdbS accumulation does not involve direct interactions between the two proteins.

Interestingly, the 11 proteins enriched in the CdbS-FLAG pull-down experiment include three chaperones, two co-chaperones and the DnaB helicase (Fig 4B). The remaining five enriched proteins have not previously been analyzed, and none have predicted functions in chromosome organization and protein accumulation. Because CdbA depletion causes defects in chromosome organization and a post-transcriptional upregulation of CdbS accumulation, we focused on DnaB as well as the five chaperones and co-chaperones.

DnaB (Mxan_5084) is the single replicative DNA helicase in *M. xanthus* and is essential for replication initiation [36]. To test whether CdbS and DnaB interact genetically, we first used the temperature-sensitive dnaBA116V mutant, which grows like WT at the permissive temperature but only completes ongoing rounds of DNA replication at the non-permissive temperature at 37°C, and then arrests replication [36]. At 32°C, WT and the *dnaB*^{A116V} mutant had similar cell lengths and similar chromosome organization patterns (S4A Fig). At 12hrs at 37°, cells of both strains had elongated, but WT cells had mostly well-organized chromosomes, while the *dnaB*^{A116V} mutant had highly condensed nucleoids centered around midcell and ParB-YFP clusters irregularly localized along the condensed nucleoids (S4A Fig). This chromosome organization differs significantly from the phenotype caused by elevated CdbS levels, with the more decondensed nucleoids organized along the cell length.

Secondly, we analyzed the *ori*/*ter* ratio in cells conditionally overexpressing *cdbS-FLAG* from P_{van}. Cephalexin-treated WT cells served as a control for elongated cells with normal replication. WT and the *cdbS-FLAG* overexpression strain had no significant differences in their *ori*/*ter* ratios neither in the absence of vanillate nor in the presence of cephalexin (for 8hrs)/vanillate (for 24hrs) (S4B Fig), supporting that a strain with an elevated CdbS level replicates as WT and that an elevated CdbS level neither inhibits nor stimulates DnaB function. Finally, we used a BACTH analysis with full-length CdbS and DnaB to test for direct interactions. While homo-hexameric DnaB [37], as expected, self-interacted, we did not detect an interaction between CdbS and DnaB (S4C Fig). Thus, how CdbS and DnaB might be connected remains unclear.

The five chaperones and co-chaperones enriched in the CdbS-FLAG pull-down experiments include two DnaK proteins, an Hsp20 protein, a J-domain protein and a GrpE homolog. DnaK proteins, called Hsp70 proteins, are ATP-dependent chaperones that interact directly with their clients. In this way, DnaK proteins contribute to the stability of clients by promoting their *de novo* folding, refolding, or solubilization of aggregates; alternatively, DnaK proteins can also target clients for degradation [38]. DnaK proteins function with two co-chaperones: J-domain proteins bind client proteins and transfer them to the partner DnaK protein, thereby also stimulating DnaK ATPase activity; GrpE proteins are nucleotide exchange factors that stimulate ADP for ATP exchange by their partner DnaK proteins [38]. DnaK proteins also work with small heat shock proteins, e.g. proteins of the Hsp20 family, which are ATP-independent chaperones that bind unfolded or misfolded proteins and transfer them to ATP-dependent chaperones, including DnaK proteins [38].

The DnaK proteins Mxan_3778 and Mxan_6605, which we renamed to CsdK1 and CsdK2 (CdbS stabilizing DnaK1 and -2, respectively (see below)), are two of 15 *M. xanthus* DnaK proteins. Both contain an N-terminal PilZ domain and the three core regions of DnaK proteins, i.e. the nucleotide-binding domain, followed by the short conserved linker and the substrate-binding domain (Fig 4C). The CsdK1 PilZ domain lacks the first half of the bipartite c-di-GMP binding motif, while the CsdK2 PilZ domain has the fully conserved c-di-GMP binding motif (Fig 4C), supporting that only this protein might bind c-di-GMP. The nucleotide-binding domains in CsdK1 and CsdK2 show high conservation, while the substrate-binding domains are more diverse (S5 Fig). In the systematic analysis of PilZ domain-containing proteins in *M. xanthus*, CsdK1 and CsdK2 were shown to be dispensable for viability, motility, exopolysaccharide synthesis and development [23].

The DnaJ protein Mxan_0750, which we renamed to DnaJ1, is one of 16 *M. xanthus* J-domain proteins. DnaJ1 contains both the characteristic J-domain and the Gly/Cys-rich

DnaJ_C domain, similar to the canonical DnaJ protein of *Escherichia coli* (Fig 4C; S6 Fig) [38]. Mxan_6672 is one of two *M. xanthus* GrpE proteins and was identified in previous work, named GrpS and is dispensable for viability and T4P-dependent motility [39]. GrpS contains the conserved GrpE domain (Fig 4C; S7 Fig). Mxan_1092, which we renamed Hsp20_1, is one of three *M. xanthus* Hsp20 domain proteins and, similarly to IbpA of *E. coli*, only contains the Hsp20 domain (Fig 4C; S8 Fig).

To test genetically whether the five chaperones and co-chaperones are important for the cellular response to CdbA depletion, we generated in-frame deletions of *csdK1*, *csdK2*, *dnaJ1*, *grpS* and *hsp20_1* in the vanillate-dependent CdbA-mCh depletion strain. All five mutations were readily obtained in the presence of vanillate; however, none of the five deletion strains were viable upon CdbA-mCh depletion (Fig 4D). Remarkably, the Δ*csdK1*Δ*csdK2* double mutant was viable upon CdbA-mCh depletion, similar to cells with the Δ*cdbS* mutation upon CdbA-mCh depletion (Fig 4D). Thus, CsdK1 and CsdK2 function redundantly during CdbA depletion and the lack of both proteins, similar to the lack of CdbS, suppresses the lethal CdbA-mCh depletion phenotype.

To test whether CdbS interacts directly with CsdK1 and/or CsdK2, we used a BACTH analysis with full-length CdbS, CsdK1 and CsdK2. We observed an interaction between CdbS and CsdK2 but not between CdbS and CsdK1 (Fig 4E). In a detailed BACTH analysis, CdbS and the non-c-di-GMP binding CdbS^{R9A} variant interacted with the DnaK part of CsdK2 but not with the CsdK2 PilZ domain (Fig 4F). Similarly, the Arg38Ala substitution in the c-di-GMP binding motif in the CsdK2 PilZ domain in the context of either the full-length protein or the PilZ domain did not interfere with the CdbS/CsdK2 interaction (Fig 4F).

These observations support that CdbS, independently of c-di-GMP binding, is a client of CsdK2. Because cells of the Δ*csdK1*Δ*csdK2* double mutant are viable upon CdbA-mCh depletion while cells with the individual deletions are not, we speculate that CdbS is also a client of CsdK1 and that the CdbS/CsdK1 interaction is of too low affinity to be detected in the BACTH analysis. This notion agrees with the CdbS-FLAG pull-down experiments in which CsdK2 was more highly enriched than CsdK1 (Fig 4B).

It remains possible that DnaJ1 and GrpS are co-chaperones of CsdK1 and/or CsdK2 and were enriched in the CdbS-FLAG pull-down experiments because they interact with CsdK1 and/or CsdK2. It is also possible that CbdS interacts directly with GrpS. Similarly, Hsp20_1 might interact directly with CdbS or CsdK1 and/or CsdK2. The observation that the Δ*dnaJ1*, Δ*grpS* and Δ*hsp20_1* mutations do not suppress the lethal CdbA-mCh depletion phenotype, suggest that if DnaJ1, GrpS and Hsp20_1 function together with CdbS, CsdK1 and/or

CsdK2, then other J-domain protein(s), the second GrpE homolog and other small heat shock proteins can take over their function.

CsdK1 and CsdK2 stabilize CdbS during CdbA depletion

To investigate how the Δ*csdK1* and Δ*csdK2* mutations jointly suppress the lethal CdbA depletion phenotype, we determined the accumulation of CdbS-FLAG in their presence or absence in a strain in which CdbS-FLAG was synthesized from the native site. CdbS-FLAG accumulated at the same level independently of the two CsdK proteins in the presence of CdbA (Fig 5A). Moreover, all four strains had cell lengths and chromosome organization as WT (S9 Fig). Upon CdbA-mCh depletion without either CsdK1 or CsdK2, the CdbS-FLAG level increased ~4-fold, and cells had aberrant lengths and chromosome organization (Fig 5BC). By contrast, in the absence of both CsdK1 and CsdK2, CdbS-FLAG only accumulated at an ~1.6-fold higher level upon CdbA-mCh depletion, cells only had a slight, although significant, increase in cell length, and most cells had WT-like chromosome organization (Fig 5BC). These findings agree with the observation that cells depleted of CdbA-mCh and lacking CsdK1 and CsdK2 are viable (Fig 4D).

Hence, CsdK1 and CsdK2 are not important for CdbS-FLAG accumulation in the presence of CdbA, but they act redundantly during CdbA-depletion to enable the increased CdbS accumulation. Because this increased CdbS accumulation is post-transcriptionally regulated, we suggest that these two DnaK chaperones stabilize CdbS during CdbA depletion rather than increasing the translation of the *cdbS* mRNA.

CdbA-depletion causes increased *csdK1* and *csdK2* transcription and accumulation

To investigate how CsdK1 and CsdK2 enable the increased CdbS accumulation in response to CdbA depletion, we analyzed the expression of *csdK1* and *csdK2* and the accumulation of CsdK1 and CsdK2. In RT-qPCR experiments, *csdK1* and *csdK2* were expressed at ~1.6- and 2.4-fold higher levels, respectively upon CdbA-mCh depletion for 24hrs (Fig 5D). Consistently, the tagged CsdK1-mVenus (from here on CsdK1-mV) and CsdK2-HA variants expressed from their native sites accumulated at ~1.6- and 1.8-fold higher levels upon depletion of CdbA-mCh for 24hrs (Fig 5EF). In published CdbA-FLAG ChIP-seq data [11], the two CdbA binding sites closest to *csdK1* are centered at -1976 and +382 relative to the transcription start site at +1, and the two sites closest to *csdK2* are centered at -2 and >3500bp away from the transcription start site at +1 (S10 Fig). These observations agree with previous findings that CdbA, even when a binding site is located in a promoter region, only moderately affects transcription [11].

These data support a pathway in which CdbA-mCh depletion alleviates the slight repression of *csdK1* and *csdK2* transcription, resulting in increased CsdK1 and CsdK2 levels that, in turn, stabilize CdbS, thereby enabling its increased accumulation and CdbS toxicity.

CdbS accumulation increases and accelerates cell death during heat stress

Our genetic analyses establish a pathway for how CdbA depletion results in increased CdbS accumulation with detrimental consequences to cell viability. However, the physiological function of this system is not clear. To address this question, we considered that under the conditions tested, cells lacking CdbS, CdbA and CdbS, or CsdK1 and CsdK2 have no evident differences to WT. We, therefore, speculated that an increased CdbS accumulation reflects the active state of the CdbA/CsdK1/CsdK2/CdbS system. Consequently, we searched for environmental stresses that activate the system using increased CdbS accumulation as a readout for activation. We focused on starvation, temperature and osmotic stress as well as DNA damaging agents because (1) the c-di-GMP level increases 10-fold during development and CdbA, CdbS and possibly CsdK2 bind c-di-GMP, (2) DnaK chaperones are important for protein refolding and stability during environmental stress, and (3) chromosome organization is disturbed by increased CdbS levels.

Using the strain synthesizing CdbS-FLAG from the native site, we found that the CdbS-FLAG level decreased during development (S11A Fig). This observation agrees with neither CdbS, CsdK1 nor CsdK2 being required to complete development [23]. When exposed to different stresses for 18hrs, cells only accumulated CdbS-FLAG at an increased level in response to growth at 37°C (*M. xanthus* is conventionally grown at 32°C) but at a reduced level in response to other stresses tested (S11B Fig).

Next, we monitored CdbS-FLAG, CdbA-mCh, CsdK1-mV, and CsdK2-HA accumulation as a function of time at 37°C using strains that synthesized these proteins from the native sites (Fig 6A). CdbS-FLAG, CsdK1-mV and CsdK2-HA levels increased over time ~3.3-fold, ~1.6-fold and ~2.0-fold compared to 32°C peaking at 8-18hrs, 8-18hrs and 12-24hrs, respectively. The CdbA-mCh level did not significantly change. Notably, the increased CdbS-FLAG accumulation depended on CsdK1 and CsdK2, and in their absence, CdbS-FLAG only accumulated at a slightly, but significantly, ~1.7-fold higher level at 18hrs at 37°C (Fig 6A). These protein accumulation profiles are strikingly similar to those observed in response to CdbA depletion.

Consistent with the similarities in the protein accumulation profiles, WT in suspension culture at 37°C had a lower growth rate than at 32°C and eventually ceased growth at ~24hrs, followed by a decrease in OD_{550}, indicating cell lysis (Fig 6B). Moreover, WT increased in

cell length at 37°C and at 18hrs and later, it had disrupted chromosome organization (Fig 6CD). At 24hrs, many WT cells had lysed, and a significant fraction of cells neither had a DAPI-stained nucleoid nor ParB-YFP clusters indicating extensive chromosome break-down (Fig 6DE). By contrast, the Δ*cdbS* and Δ*csdK1*Δ*csdK2* mutants at 37°C initially had the same growth rate as at 32°C, and only ceased growth at ~36hrs followed by a decrease in OD_{550} (Fig 6B). Consistently, they had a less severe filamentation phenotype and no defects in chromosome organization at ~24hrs, and only displayed disrupted chromosome organization and cell lysis lyse at ~36hrs at 37°C (Fig 6DE). In agreement with these observations, all three strains had a three-log defect in plating efficiency at 37°C compared to 32°C (Fig 6B). Finally, a strain expressing the non-c-di-GMP binding $CdbS^{R9A}$-FLAG variant phenocopied the WT strain at 37°C (S12A-D Fig). Hence, 37°C is a lethal growth temperature for *M. xanthus,* and the increased CdbS level mediated by the two CsdK proteins acts during heat stress to accelerate cell death independently of c-di-GMP binding.

Interestingly, the CdbA-mCh level did not decrease at 37°C (Fig 6A). CdbA-mCh co-localized with the nucleoid at both temperatures without evident differences (S13A Fig). Because c-di-GMP and DNA binding by CdbA are mutually exclusive *in vitro* [11], we speculated that an increase in the cellular c-di-GMP level at 37°C could curb DNA binding by CdbA. Consequently, we determined the cellular level of c-di-GMP at 32°C and 37°C. Intriguingly, the c-di-GMP level had increased ~4-fold at 8hrs coinciding with the onset of the increased accumulation of CdbS, CsdK1 and CsdK2 (Fig 6F). At 18hrs, the c-di-GMP level had returned to the level at 32°C.

Paradoxically, CdbS, CsdK1 and CsdK2 contribute to cell death in cells maintained at 37°C ≥24hrs. We speculated that these three proteins could contribute a protective function if cells were incubated for shorter periods at 37°C. To test this idea, WT and Δ*cdbS* cells were incubated at 37°C for up to 12hrs and then plated at 32°C. The WT and Δ*cdbS* strains progressively lost viability at 37°C and had the same recovery efficiency at all time points (S13B Fig).

Discussion

Here we investigated the mechanism underlying the essentiality of the c-di-GMP binding NAP CdbA in *M. xanthus*. We demonstrate that the loss of function of *cdbS*, which encodes a stand-alone PilZ domain protein, completely alleviates the toxicity of the lack of CdbA. Accordingly, CdbA depletion in the presence of CdbS disrupts chromosome organization resulting in inhibition of cell division, cell elongation and, eventually, cell death. By contrast,

in the absence of CdbA and CdbS, chromosome organization is not disrupted, and cells are fully viable. Thus, CdbS is the critical factor during CdbA depletion that mediates the disrupted chromosome organization, resulting in cellular filamentation and cell death.

Four key observations indicate a genetic pathway for the link between CdbA and CdbS. First, upon CdbA depletion, CdbS accumulation is upregulated ~4-fold post-transcriptionally. Second, while the two DnaK chaperones CsdK1 and CsdK2 are not important for CdbS accumulation in the presence of CdbA, the ~4-fold increase upon CdbA depletion depends on the redundant activities of CsdK1 and CsdK2. Third, upon CdbA depletion, *csdK1* and *csdK2* transcription increases ~1.6-2.4-fold and, accordingly, the CsdK1 and CsdK2 levels increase ~1.6-1.8-fold. Fourth, a ~4-fold increased CdbS level in the presence of CdbA phenocopies CdbA depletion. These results support a genetic pathway in which CdbA depletion alleviates the slight transcriptional repression of *csdK1* and *csdK2,* resulting in slightly increased CsdK1 and CsdK2 levels. The increased CsdK1 and CsdK2 levels, in turn, stabilize CdbS resulting in its increased accumulation. Finally, this ~4-fold increased CdbS accumulation is sufficient for causing disrupted chromosome organization, cellular filamentation and cell death.

Because this genetic pathway is based on gene knock-outs and, thus, the complete loss of function of individual proteins, it could be argued that the effects observed upon CdbA depletion represent an aberrantly activated or overactivated CdbA/CsdK1/CsdK2/CdbS system that may not normally occur in cells [40]. Therefore, we searched for physiological cue(s) that could induce the CdbA/CsdK1/CsdK2/CdbS system. Indeed, the growth of *M. xanthus* at 37°C (as opposed to the conventional growth temperature at 32°C) caused increased CsdK1 and CsdK2 accumulation, which, in turn, mediated an increased CdbS accumulation. At this temperature, the increased CdbS level contributed to disrupted chromosome organization, cell elongation and cell death. Importantly, at 37°C, the CdbA accumulation level did not decrease, raising the question of how the CsdK1 and CsdK2 levels increase. Interestingly, we found that the cellular c-di-GMP level increased at 37°C, coinciding with the onset of the increased accumulation of CdbS, CsdK1 and CsdK2. These observations support the attractive idea that an increased c-di-GMP level at 37°C could curb DNA binding by CdbA, thereby alleviating the repression of *csdK1* and *csdK2* transcription. Of note, at 32°C, a *M. xanthus* strain with a c-di-GMP level artificially increased ~7-fold has no defects in chromosome organization, growth and viability [11, 20]. Thus, it remains possible that an increased c-di-GMP level at 37°C is sufficient to curb CdbA DNA binding but not at 32°C. Alternatively, the increased accumulation of the two CsdK proteins at 37°C is independent of CdbA or the increased c-di-GMP level functions with a yet-to-be-identified mechanism at 37°C.

Altogether, our data support two pathways for activating the CdbA/CsdK1/CsdK2/CdbS system. First, in the absence of CdbA, *csdK1* and *csdK2* transcription increases, resulting in increased CsdK1 and CsdK2 levels that stabilize CdbS, thereby enabling its increased accumulation and toxicity. Second, in response to exposure to 37°C, and possibly involving curbed CdbA DNA binding caused by an increased c-di-GMP level, CsdK1 and CsdK2 levels increase, enabling CdbS stabilization, and thereby its increased accumulation and toxicity.

Paradoxically, the CdbA/CsdK1/CsdK2/CdbS system contributes to cell death in both pathways, raising the question of this system's physiological function. Generally, a stress response induced by an environmental cue contributes to cellular homeostasis, i.e. after induction by a specific cue, the induced system facilitates cellular adaption to this cue, thereby increasing cellular fitness, and is then switched off. We, therefore, investigated whether the CdbA/CsdK1/CsdK2/CdbS system provides a protective function at 37°C if cells are only incubated for short periods at 37°C, and then returned to 32°C. Under these conditions, WT and Δ*cdbS* cells behaved similarly and progressively lost viability, indicating that the CdbA/CsdK1/CsdK2/CdbS system does not evidently contribute to cellular homeostasis and fitness. As such, the CdbA/CsdK1/CsdK2/CdbS system is reminiscent of toxin/antitoxin systems, in which CdbS would be the toxin. Typically, toxin/antitoxin systems consist of two adjacent genes that encode a toxin that causes growth arrest or cell death and a partner antitoxin that counteracts the toxin by direct interaction [41, 42]. However, CdbA, CsdK1, CsdK2 and CdbS are not encoded by flanking genes and with the exception of CdbS and CsdK2, and possibly CsdK1, there is no evidence supporting that they interact. We, therefore, suggest that the CdbA/CsdK1/CsdK2/CdbS system is a system for regulated cell death upon CdbA depletion and contributes to cell death upon heat stress at 37°. This function would be analogous to a recently described cytoplasmic contractile injection system in *Streptomyces coelicolor* that contributes to regulated cell death in response to different stresses [43, 44].

We confirmed that *M. xanthus* cells elongate when grown at 37°C [45-47]; however, in these previous experiments, cells were only followed for 12-18hrs at this temperature. A surprising finding from our investigations is that under our conditions, 37°C is a lethal growth temperature for *M. xanthus* independently of CdbS. However, the CdbA/CsdK1/CsdK2/CdbS system accelerates cell death at 37°C.

CdbA depletion causes disrupted chromosome organization that, in turn, inhibits cell division causing cellular filamentation and cell death. Here we show that these effects of CdbA depletion depend on CdbS. In other words, it is not the lack of CdbA that causes the massive defects in chromosome organization; the increased CdbS level causes these

557 defects. Because CdbA binds >550 sites on the *M. xanthus* chromosome with moderate
558 sequence specificity, is highly abundant and has only minor effects on transcription (here;
559 [11]), CdbA fulfils the criteria for being a NAP [15-17]. Equally, the observation that DNA
560 binding and c-di-GMP binding are mutually exclusive [11] supports that DNA binding is
561 modulated by c-di-GMP [11]. However, the essential function of CdbA is to maintain the
562 CdbS level appropriately low.

563 How, then, does a high CdbS level disrupt chromosome organization? Lack of CdbS in the
564 presence or absence of CdbA affects neither the chromosome nor viability. Thus, CdbS is
565 not essential for these two processes. In CdbS-FLAG pull-down experiments, the
566 replicative DnaB helicase was enriched. However, our results do not provide support for a
567 direct interaction between CdbS and DnaB. Interestingly, the PlzA protein of *Borrelia*
568 *burgdorferi*, which consists of two PilZ domains connected by a short linker that binds c-di-
569 GMP [48], was reported to bind DNA and RNA in a c-di-GMP-dependent manner [49]. As
570 opposed to PlzA [49], CdbS consists of a single PilZ domain, and its function is
571 independent of c-di-GMP binding. Nevertheless, it remains possible that CdbS could be a
572 DNA/RNA-binding protein, thereby contributing to chromosome organization. The two main
573 contributors to chromosome organization and segregation in *M. xanthus*, i.e. the ParABS
574 system and SMC, are essential at 32°C [29, 33]. Thus, it is also possible that increased
575 CdbS levels interfere with the functioning of one or both of these systems. It will be
576 important to address whether CdbS binds DNA/RNA in the future. Also, the pull-down
577 experiments with CdbS-FLAG were conducted under conditions where CdbS was not
578 overaccumulating (and, thus, not toxic). Therefore, seeking potential interaction partners
579 under conditions where CdbS is overaccumulating and toxic to cells will also be important.

580 The two DnaK proteins CsdK1 and CsdK2 function redundantly to mediate the increased
581 CdbS accumulation in response to CdbA depletion and exposure to 37°C. These
582 observations, taken together with the results of the CdbS-FLAG pull-down experiments and
583 BACTH analyses in which CdbA interacts with the core DnaK regions of CsdK2 but not with
584 the CsdK2 PilZ domain, support that CdbS is a client of CsdK1 and CsdK2. CsdK1 and
585 CsdK2 are only important for the increased accumulation in response to CdbA depletion and
586 heat stress at 37°C but not for CdbS accumulation in the presence of CdbA at 32°C.
587 Because the increased accumulation in response to CdbA depletion is regulated post-
588 transcriptionally, we suggest that the two CsdK proteins stabilize CdbS upon CdbA depletion
589 and heat stress at 37°C, likely by stimulating correct folding of CdbS.

590 Among the four CdbA/CsdK1/CsdK2/CdbS system proteins, CdbA and CdbS are verified c-
591 di-GMP binding proteins, and the CsdK2 PilZ domain likely binds c-di-GMP. C-di-GMP and

592 DNA binding by CdbA are mutually exclusive *in vitro*; c-di-GMP binding by CdbS is not
593 important for toxicity, and it is not known whether c-di-GMP by the CsdK2 PilZ domain is
594 important for function. As described, we speculate that the increased c-di-GMP at 37°C
595 could modulate DNA binding by CdbA, thereby contributing to the increased accumulation of
596 the two CsdK proteins at 37°C. Interestingly, growth temperature has been implicated in
597 regulating the c-di-GMP level in other bacteria. A low temperature causes increased c-di-
598 GMP accumulation in *Vibrio cholerae* and *Pseudomonas putida* by unknown mechanisms
599 [50]. In *P. aeruginosa,* an increased temperature causes an increased c-di-GMP level via
600 direct activation of the thermosensitive diguanylate cyclase TdcA [51]. In the future, it will be
601 interesting to investigate the mechanism underlying the increased c-di-GMP level in
602 response to exposure of *M. xanthus* cells to 37°C and how it might contribute to cell death.

603

Materials and Methods

Strains and cell growth. All *M. xanthus* strains are derivatives of the WT DK1622 [52] and are listed in Table S2. Plasmids and primers used are listed in Table S3 and Table S4, respectively. In-frame deletions were generated as described [53]. Plasmids for ectopic expression of genes were integrated in a single copy either by site-specific recombination into the Mx8 *attB* site or by homologous recombination at the *mxan_18/19* locus. All plasmids were verified by DNA sequencing and all strains were verified by PCR. *M. xanthus* was grown at 32°C in 1% CTT broth (1% Bacto Casitone (Gibco), 10mM Tris-HCl pH 8.0, 1mM KPO_4 pH 7.6, 8mM $MgSO_4$) [54] or on 1.5% agar supplemented with 1% CTT broth, and kanamycin (50µg mL^{-1}) or oxytetracycline (10µg mL^{-1}) if relevant. Mitomycin C and nalidixic acid were added to final concentrations of 20µg mL^{-1}. Plasmids were propagated in *Escherichia coli* NEB Turbo ((F' *proA*$^+$*B*$^+$ *lacI*^{q} Δ*lacZM15/fhuA2* Δ*(lac-proAB) glnV galK16 galE15 R(zgb-210::Tn10)* Tet^S *endA1 thi-1* Δ*(hsdS-mcrB)5*)) (New England Biolabs) at 37°C in lysogeny broth (LB) [55] supplemented with kanamycin (50µg mL^{-1}), tetracycline (15µg mL^{-1}) or carbenicillin (100µg mL^{-1}).

Development. Cells were developed under submerged conditions as described [56]. Briefly, exponentially growing *M. xanthus* in CTT broth were harvested at 5,000 *g* for 5min and resuspended in MC7 buffer (10 mM 3-(*N*-morpholino)propanesulfonic acid (MOPS) pH 6.8, 1 mM $CaCl_2$) to 7×10^9 cells mL^{-1}. 50µL was added to 350µL of MC7 buffer in 24-well polystyrene plate (Falcon) and incubated at 32°C.

Whole genome sequencing. Chromosomal DNA of the eight suppressor mutants and the original strain (SA5691) was isolated using the MasterPure™ DNA Purification Kit (Epicentre Biotechnologies) according to the manufacturer's recommendation. The FS libraries were prepared and sequenced (paired-end, 2×250 bp) on an Illumina HiSeq2500 instrument at the Max Planck-Genome-Centre Cologne. CLC workbench 12.0 (Qiagen, Hilden, Germany) was used for computational processing of sequencing data.

Immunoblots. Immunoblotting was performed as described in [55]. For sample preparation, *M. xanthus* cells were harvested from suspension cultures or from cells developed under submerged conditions and resuspended in sodium dodecyl sulfate (SDS) lysis buffer. The same amount of protein was loaded per sample (30µg). After electrophoresis, proteins were transferred to a nitrocellulose membrane (Cytiva) with 0.2µm pore size using a TransBlot® Turbo™ Transfer System (Bio-Rad) with transfer buffer (300mM Tris-HCl, 300mM glycine, 0.05% (w/v) SDS, pH 9.0). As primary antibodies, rabbit polyclonal α-FLAG (1:2,000, Rockland), α-mCherry (1:2500, BioVision), α-HA (1:2000, Sigma) and α-PilC (1:2000) [57] were used with horseradish-peroxidase-conjugated α-rabbit immunoglobulin G (1:15000,

Sigma) as secondary antibody. α-GFP (1:2000, Sigma) primary antibodies were used together with horseradish peroxidase-conjugated α-mouse immunoglobulin G (1:5000, GE Healthcare) as secondary antibody. α-polyHistidine antibodies conjugated with peroxidase (1:2000, Sigma) were used to detect His_6-tagged proteins. Immunoblots were developed using Immobilon® Forte Western HRP Substrate (Millipore) on a LAS-4000 imager (Fujifilm). The signal intensities of the individual bands were quantified using Fiji [58]. Each band intensity of the protein of interest was normalized relative to the intensity of the respective PilC loading control, mean ± STDEV were calculated from three independent biological replicates.

RT-qPCR. Total RNA from *M. xanthus* cells grown on 1.5% agar supplemented with 1% CTT broth was extracted using the Monarch Total RNA Miniprep Kit (New England Biolabs). Briefly, 10^9 cells were scraped off the agar-plates and resuspended in 200µL lysis-buffer (100mM Tris-HCl pH 7.6, 1mg mL^{-1} lysozyme), and incubated at 25°C, 5min. RNA purification was performed according to manufacturer's protocol. DNA was removed using Turbo DNase (Thermo Fisher Scientific) and DNase was removed using the Monarch RNA Cleanup Kit (50 µg; New England Biolabs). LunaScript RT SuperMix Kit (New England Biolabs) was used to generate cDNA using 1µg RNA. qPCR reactions were performed on an Applied Biosystems 7500 Real-Time PCR system using the Luna Universal qPCR MasterMix (New England Biolabs) with the primers listed in Table S4. *rpsS*/*mxan_3303*, which encodes the small ribosomal subunit protein S19, was used as an internal control [59]. Data analysis was performed using the comparative C_T method [60].

Microscopy. Fluorescence microscopy was performed as described [11]. Briefly, exponentially growing cells were stained with 1mg mL^{-1} DAPI for 10min at 32°C, transferred to a pad containing 1.5% agarose (Cambrex) with TPM buffer (10 mM Tris-HCl pH 7.6, 1 mM KPO_4 pH 7.6, 8 mM MgSO4) supplemented with 0.2% CTT broth on a microscope slide, and covered with a coverslip. A Leica DMi8 inverted microscope was used for imaging, and phase contrast and fluorescence snapshots were acquired using a Hamamatsu ORCA-flash V2 Digital CMOS camera. For image processing, Metamorph v 7.5 (Molecular Devices) was used. Using a custom made Matlab R2020a (MathWorks) script, cells and fluorescent signals were detected automatically using Oufti48 [61].

Determination of *ori*/*ter* ratio. To determine the *ori*/*ter* ratio, chromosomal DNA was isolated as described. The *ori* region was amplified using the primer pairs ori 1/dnaA fwd with ori 1/dnaA rev and ori 2/7483 fwd with ori 2/7483 rev, while the *ter* region was amplified using the primer pair 3778_ter 1 qPCR fwd with 3778_ter 1 qPCR rev and the Luna Universal

673 qPCR Master Mix (New England Biolabs). Quantification of the *ori*/*ter* ratio was performed
674 using the the $2^{-\Delta CT}$ method as described [62].

675 Protein purification. To purify His_6-CdbS and His_6-$CdbS^{R9A}$, *E.coli* Arctic Express (DE3) RP
676 (Agilent Technologies) was transformed with pMS007 and pMS008, respectively. Cultures
677 were grown in 2L LB with gentamycin and kanamycin to an OD_{600} of 0.5 to 0.7 at 30°C.
678 Protein overproduction was induced by adding isopropyl-β-D-1-thiogalactopyranoside (IPTG)
679 to a final concentration of 0.5 mM, and then the culture was grown at 11°C for 24hrs. Cells
680 were harvested by centrifugation at 3,800 *g* for 30min at 4°C. The pellet was resuspended in
681 25mL Lysis Buffer (50mM Tris-HCl pH 7, 150mM NaCl, 10% (v/v) glycerol, 1mM ß-
682 mercaptoethanol, 10mM imidazole, cOmplete protease inhibitor EDTA-free (Roche
683 Diagnostics GmbH)) and sonicated for 30min with a UP200St sonifier (60% pulse, 50%
684 amplitude, 30sec on/off time; Hielscher) on ice. The solution was centrifuged at 48,000 *g* at
685 4°C for 45min at 4°C. The soluble fraction was loaded onto a 5ml HiTrap Chelating HP
686 column (GE Healthcare) that had been pre-loaded with $NiSO_4$ according to the
687 manufacturer's recommendation and pre-equilibrated with wash buffer (50mM Tris-HCl pH 7,
688 150mM NaCl, 10% (v/v) glycerol, 1mM 1mM ß-mercaptoethanol, 20mM imidazole). The
689 column was washed with 10 column volumes wash buffer. Proteins were eluted with elution
690 buffer (50mM Tris-HCl pH 7, 150mM NaCl, 10% (v/v) glycerol, 1mM ß-mercaptoethanol,
691 500mM imidazole) with a linear imidazole gradient from 50 to 500mM. Fractions containing
692 the protein of interest were combined and mixed with anion exchange buffer A (50mM Tris-
693 HCl pH 7, 10% (v/v) glycerol, 1mM ß-mercaptoethanol) in a 1:3 ratio and then loaded onto a
694 5 ml HiTrap SP HP (GE Heathcare) column. Bound protein was eluted along a 5 column
695 volume gradient of anion exchange buffer B (50mM Tris-HCl pH 7, 10% (v/v) glycerol, 1mM
696 ß-mercaptoethanol, 2M NaCl). Fractions containing the protein of interest were pooled and
697 concentrated using an Amicon® Ultra-4 3K centrifugal filter unit (Merck) according to the
698 manufacturer's recommendation, while the buffer was exchanged to dialysis buffer (50mM
699 Tris-HCl pH 7, 150mM NaCl, 10% (v/v) glycerol). Purified protein aliquots were shock-frozen
700 in liquid nitrogen and stored at -80°C.

701 Bio-layer interferometry. Bio-layer interferometry was performed using the BLItz system
702 (forteBio) as described [12]. 500nM biotinylated c-di-GMP (Biolog) in dialysis buffer
703 supplemented with 0.02% (wt/vol) Tween-20 was loaded onto a Streptavidin SA biosensor
704 (forteBio) for 120sec followed by 30sec of washing with dialysis buffer. To calculate binding
705 kinetics, varying concentration of the protein of interest in dialysis buffer supplemented with
706 0.02% (wt/vol) Tween-20 was applied to the biosensor for 120sec followed by 120sec of
707 dissociation with dialysis buffer.

Determination of c-di-GMP level. The c-di-GMP level was determined as described [24]. Briefly, cultures were harvested at 2,500 *g* for 20min at 4°C. After lysing cells in extraction buffer (high-pressure liquid chromatography [HPLC]-grade acetonitrile-methanol-water [2/2/1, vol/vol/vol]), the supernatants were evaporated to dryness in a vacuum centrifuge. Subsequently, the pellets were dissolved in HPLC-grade water and analyzed by liquid chromatography-tandem mass spectrometry (LC-MS/MS). The c-di-GMP level was measured at the Research Service Centre Metabolomics at the Hannover Medical School, Germany.

In vivo pull-down and label-free mass spectrometry-based quantitative proteomics. Exponentially growing cultures were harvested by centrifugation at 2,500 *g* at 20°C for 10min. The pellet was resuspended in 10ml HNN buffer (50mM HEPES pH 7.2, 150mM NaCl, 5mM EDTA, cOmplete protease inhibitor (Roche Diagnostics GmbH), 0.5% (v/v) NP40) and sonicated for 1min with a UP200St sonifier (60% pulse, 50% amplitude; Hielscher) on ice. To each sample, 10µl anti-FLAG® M2 magnetic beads (Merck) were added. Next, the samples were placed in an overhead rotor for 90min at 4°C. The supernatant was removed and the beads were washed with HNN buffer followed by four times washing with 100mM ammoniumbicarbonate to remove all detergent and protease inhibitors. Further sample processing was carried out as described [63]. Briefly, enriched proteins were eluted by adding 1µg trypsin (Promega) and incubation for 30min at 30°C, and further incubated overnight in the presence of 5mM Tris(2-carboxyethyl)phosphin (TCEP). Following, acetylation using 10mM iodoacetamide for 30min at 25°C in the dark, the peptides were desalted using C18 solid phase extraction. Liquid chromatography-mass spectrometry (LC-MS) analysis of the peptide samples were carried out on a Q-Exactive Plus instrument connected to an Ultimate 3000 RSLCnano and a nanospray flex ion source (all Thermo Scientific). Peptide separation was performed on a C18 reverse phase HPLC column (75µm × 42cm; 2.4µm, Dr. Maisch). The peptides were loaded onto a PepMap 100 precolumn (Thermo Scientific) and eluted by a linear acetonitrile (ACN) gradient from 6-35% solvent B over 30min (solvent A: 0.15% formic acid; solvent B: 99.85% ACN in 0.15% formic acid) with 300nL min^{-1} flow rate. The spray voltage was set to 2.5kV, and the temperature of the heated capillary was set to 300°C. Survey full-scan MS spectra (m/z = 375-1500) were acquired in the Orbitrap with a resolution of 70,000 (at m/z 200) after accumulation a maximum of 3×10^6 ions in the Orbitrap. Up to 10 most intense ions were subjected to fragmentation using high collision dissociation (HCD) at 27% normalized collision energy. Fragment spectra were acquired at 17,500 resolution. The ion accumulation time was set to 50ms for both MS survey and MS/MS scans. The charged state screening modus was

743 enabled to exclude unassigned and singly charged ions. The dynamic exclusion duration
744 was set to 30sec.

745 Label-free quantification of the samples was performed using MaxQuant (Version 1.6.10.43)
746 [64]. For Andromeda database searches implemented in the MaxQuant environment, a *M.*
747 *xanthus* Uniprot protein database (downloaded in 10/2016) was used. The search criteria
748 were set as follows: full tryptic specificity was required (cleavage after lysine or arginine
749 residues); two missed cleavages allowed; carbamidomethylation (C) was set as fixed
750 modification; oxidation (M) and deamidation (N, Q) as variable modification. MaxQuant was
751 operated in default settings without the “Match-between-run” option. For protein
752 quantification, iBAQ values (intensity-based absolute quantification) were calculated within
753 MaxQuant [65]. Calculated iBAQ values were normalized to iBAQ-protein sum of all detected
754 proteins. Student’s t-test was performed within Perseus [66] with the following parameters
755 (FDR: 0.01, s0: 0.5).

756 The proteomics data have been deposited to the ProteomeXchange consortium via the
757 PRIDE partner repository [67] with the dataset identifier PXD041344 (Username:
758 reviewer_pxd041344@ebi.ac.uk; password: iCibsHnr).

759 Bioinformatics. The structural model of CdbS was generated using AlphaFold via ColabFold
760 [68, 69] using the Alphafold2_mmseqs2 notebook with default settings, except recycles were
761 set to six; figure of protein model was generated using PyMOL (Schrödinger LLC). Predicted
762 Local Distance Difference Test (pLDDT) and predicted Alignment Error (pAE) graphs of the
763 five models generated by Alphafold2_mmseqs2 notebook were made using a custom made
764 Matlab R2020a (The MathWorks) script. Ranking of the models was performed based on
765 combined pLDDT and pAE values, with the best-ranked model used for further analysis and
766 presentation. Protein domains were predicted with HMMER [70]. Alignments and
767 phylogenies were constructed using MEGA-X [71]. Similarity and identity between proteins
768 were analyzed with EMBOSS Needle [72].

769 Plasmid construction: Genomic *M. xanthus* DNA or plasmids were used as templates to
770 amplify genes and genomic regions of interest.

771 pMS007 and pMS008 are derivatives of pET28a(+): *cdbS* was amplified from genomic DNA
772 using primers 4328 fw_NdeI and oMS004. To generate the *cdbS*^{R9A} allele, *cdbS* was
773 amplified from genomic DNA using the primers oMS002 and oMS004. The resulting
774 fragment was used as a template for another PCR and amplified using the primers 4328
775 fw_NdeI and oMS004. Both inserts were inserted into pET28a(+)via the NdeI/HindII sites.

776 pMS018 is a derivative of pBJ114: To amplify the upstream fragment, the primers oMS024
777 and oMS013 were used using genomic DNA. To generate the downstream fragment, the
778 primer pairs oMS025 and oMS087 were used. The final fragment was obtained via overlap
779 PCR and inserted into pBJ114 via the HindIII/EcoRI sites.

780 pMS024 and pMS026 are derivatives of pMR3691: To amplify FLAG-tagged *cdbS*, the gene
781 was amplified using the primers 4328 fw_NdeI and oMS041 from SA10217. The fragment
782 was inserted into pMR3691 via the NdeI/EcoRI sites. To amplify the *cdbS*^{R9A} allele, the
783 primer pairs oMS002 and oMS041 were used with pMS024 as a template. The resulting
784 fragment was used for another PCR using 4328 fw_NdeI and oMS041 as primers. This final
785 fragment was inserted into pMR3691 via the NdeI/EcoRI sites.

786 pMS054 is a derivative of pBJ114: To amplify the upstream fragment, primers oMS082 and
787 oMS083 were used with genomic DNA. To amplify the mCherry fragment, the primer pairs
788 oMS084 and oMS085 were used using SA5691 as a template. These two fragments were
789 ligated via the BamHI site. To generate the downstream fragment, the primer pairs oMS086
790 and oMS087 were used with genomic DNA as a template. The final fragment was obtained
791 via overlap PCR and inserted into pBJ114 via the HindIII/EcoRI sites.

792 pMS055: To amplify the upstream fragment, the primers oMS092 and oMS093 were used
793 using genomic DNA as a template. To generate the downstream fragment, the primer pairs
794 oMS094 and oMS095 using genomic DNA as a template. The final fragment was obtained
795 via overlap PCR and was inserted into pBJ114 via the HindIII/EcoRI sites.

796 pMS056: To amplify the upstream fragment, the primers oMS100 and oMS101 were used
797 using genomic DNA as a template. To generate the downstream fragment, the primer pairs
798 oMS102 and oMS103 using genomic DNA as a template. The final fragment was obtained
799 via overlap PCR and was inserted into pBJ114 via the HindIII/EcoRI sites.

800 pMS057 is a derivative of pBJ114: To amplify the upstream fragment, the primers oMS116
801 and oMS117 were used using genomic DNA as a template. To generate the downstream
802 fragment, the primer pairs oMS118 and oMS119 using genomic DNA as a template. The
803 final fragment was obtained via overlap PCR and was inserted into pBJ114 via the
804 HindIII/EcoRI sites.

805 pMS088: To amplify the upstream fragment, the primers oMS177 and oMS231 were used
806 using genomic DNA as a template. To amplify the mVenus fragment, the primers oMS194
807 and oMS232 were used with pFM60 (gift of Franziska Müller) as template. To generate the
808 downstream fragment, the primer pairs oMS228 and oMS180 using genomic DNA as a
809 template. The upstream fragment and the mVenus fragment were fused via overlap PCR,

before the resulting fragment was fused to the downstream fragment via a second overlap PCR. This final fragment was inserted into pBJ114 via the HindIII/EcoRI sites.

pMS089: To amplify the upstream fragment, the primers oMS182 and oMS183 were used using genomic DNA as a template. To generate the downstream fragment, the primer pairs oMS184 and oMS185 using genomic DNA as a template. The final fragment was obtained via overlap PCR and was inserted into pBJ114 via the HindIII/EcoRI sites.

pMS102: The P_{nat}*parB-YFP* fragment was amplified from pDJS151 using the primers oMS068 and oMS211. The P_{nat}*cdbS-FLAG* fragment was amplified from genomic DNA using the primer pairs oMS212 and oMS004. The two fragments were ligated via the NdeI site, and the resulting fragment was inserted into pBJ114 via the XbaI/EcoRI sites.

BACTH plasmids were all constructed using the same strategy. For most constructs, the same fragment of each gene was amplified from genomic DNA and inserted into the respective plasmids via the XbaI/KpnI. For CdbS constructs, the primers oMS131 and oMS132 were used, while for the $CdbS^{R9A}$ variant, the template was pMS026. For CsdK1 constructs, the primers oMS133 and oMS134 were used. For DnaB constructs, the primers oMS154 and oMS155 were used. For CsdK2 constructs in pUT18C, the primers oMS135 and oMS136 were used. For the pKT25-CsdK2 construct, the primer pair oMS135 and oMS141 was used. All CsdK2 fragments were inserted into the respective vector via the XbaI/EcoRI sites.

For the $CsdK2^{R38A}$ variants, the primer pairs oMS135 and oMS204 and additionally oMS205 and oMS206 were used to amplify two fragments that were then fused using overlap PCR. The resulting fragment was cloned into the BACTH plasmids containing CsdK2 using the XbaI/XmaI sites.

For the $CsdK2^{1-435}$ variant, the primer oMS135 was used together with oMS208 for the pKT25 construct or oMS206 for pUT18C constructs. Similarly, the same primer pairs were used for the $CsdK2^{1-435\_R38A}$ variants using pUT18C-CsdK2R38A as a template. For the $CsdK2^{298-1146}$ variant, the primer oMS207 was used together with oMS141 for the pKT25 construct or oMS136 for pUT18C constructs.

Acknowledgements. We thank Penelope Higgs, Lee Kroos and Daniel Wall for helpful discussions and Anke Treuner-Lange, Sabrina Huneke and Franziska Müller for strains and plasmids. The Max Planck Society generously supported this work.

Funding. This work was funded by the Max Planck Society (to L.S.-A.).

Declaration of Interests. The authors declare no competing interests.

Author contributions

MS, DS and LSA conceptualized the study.
MS, DS and TG conducted the experimental work.
MS, DS and TG analyzed experimental data.
MS and LSA wrote the original draft of the manuscript.
MS, DS, TG and LSA reviewed and edited the manuscript.
LSA provided supervision.
LSA acquired funding.

Availability of data and materials. The authors declare that all data supporting this study are available within the article and its Supplementary Information files.

References

1. Jenal U, Reinders A, Lori C. Cyclic di-GMP: second messenger extraordinaire. Nat Rev Microbiol. 2017; 15:271-284.

2. Römling U, Galperin MY, Gomelsky M. Cyclic di-GMP: the first 25 years of a universal bacterial second messenger. Microbiol Mol Biol Rev. 2013; 77:1-52.

3. Christen M, Christen B, Allan MG, Folcher M, Jeno P, Grzesiek S, et al. DgrA is a member of a new family of cyclic diguanosine monophosphate receptors and controls flagellar motor function in *Caulobacter crescentus*. Proc Natl Acad Sci USA. 2007; 104:7729-7729.

4. Ramelot TA, Yee A, Cort JR, Semesi A, Arrowsmith CH, Kennedy MA. NMR structure and binding studies confirm that PA4608 from *Pseudomonas aeruginosa* is a PilZ domain and a c-di-GMP binding protein. Proteins. 2007; 66:266-271.

5. Merighi M, Lee VT, Hyodo M, Hayakawa Y, Lory S. The second messenger bis-(3′-5′)-cyclic-GMP and its PilZ domain-containing receptor Alg44 are required for alginate biosynthesis in *Pseudomonas aeruginosa*. Mol Microbiol. 2007; 65:876-895.

6. Ryjenkov DA, Simm R, Romling U, Gomelsky M. The PilZ domain is a receptor for the second messenger c-di-GMP: the PilZ domain protein YcgR controls motility in enterobacteria. J Biol Chem. 2006; 281:30310-30314.

7. Pratt JT, Tamayo R, Tischler AD, Camilli A. PilZ domain proteins bind cyclic diguanylate and regulate diverse processes in *Vibrio cholerae*. J Biol Chem. 2007; 282:12860-70.

8. Chin KH, Lee YC, Tu ZL, Chen CH, Tseng YH, Yang JM, et al. The cAMP receptor-like protein CLP is a novel c-di-GMP receptor linking cell-cell signaling to virulence gene expression in *Xanthomonas campestris*. J Mol Biol 2010; 396:646-662.

9. Krasteva PV, Fong JC, Shikuma NJ, Beyhan S, Navarro MV, Yildiz FH, et al. *Vibrio cholerae* VpsT regulates matrix production and motility by directly sensing cyclic di-GMP. Science. 2010; 327:866-868.

10. Tschowri N, Schumacher MA, Schlimpert S, Chinnam NB, Findlay KC, Brennan RG, et al. Tetrameric c-di-GMP mediates effective transcription factor dimerization to control *Streptomyces* development. Cell. 2014; 158:1136-1147.

11. Skotnicka D, Steinchen W, Szadkowski D, Cadby IT, Lovering AL, Bange G, et al. CdbA is a DNA-binding protein and c-di-GMP receptor important for nucleoid organization and segregation in *Myxococcus xanthus*. Nat Commun. 2020; 11:1791.

12. Schäper S, Steinchen W, Krol E, Altegoer F, Skotnicka D, Søgaard-Andersen L, et al. AraC-like transcriptional activator CuxR binds c-di-GMP by a PilZ-like mechanism to regulate extracellular polysaccharide production. Proc Natl Acad Sci U S A. 2017; 114:E4822-e4831.

13. Matsuyama BY, Krasteva PV, Baraquet C, Harwood CS, Sondermann H, Navarro MVAS. Mechanistic insights into c-di-GMP-dependent control of the biofilm regulator FleQ from *Pseudomonas aeruginosa*. Proc Natl Acad sci USA. 2016; 113:E209-E218.

14. Li W, He ZG. LtmA, a novel cyclic di-GMP-responsive activator, broadly regulates the expression of lipid transport and metabolism genes in *Mycobacterium smegmatis*. Nucl Acids Res. 2012; 40:11292–11307.

899 15. Dorman CJ, Schumacher MA, Bush MJ, Brennan RG, Buttner MJ. When is a
900 transcription factor a NAP? Curr Opin Microbiol. 2020; 55:26-33.

901 16. Badrinarayanan A, Le TB, Laub MT. Bacterial chromosome organization and
902 segregation. Annu Rev Cell Dev Biol. 2015; 31:171-99.

903 17. Dillon SC, Dorman CJ. Bacterial nucleoid-associated proteins, nucleoid structure and
904 gene expression. Nat Rev Microbiol. 2010; 8:185-95.

905 18. Konovalova A, Petters T, Søgaard-Andersen L. Extracellular biology of *Myxococcus*
906 *xanthus*. FEMS Microbiol Rev. 2010; 34:89-106.

907 19. Muñoz-Dorado J, Marcos-Torres FJ, Garcia-Bravo E, Moraleda-Munoz A, Perez J.
908 Myxobacteria: moving, killing, feeding, and surviving together. Front Microbiol. 2016; 7:781.

909 20. Skotnicka D, Petters T, Heering J, Hoppert M, Kaever V, Søgaard-Andersen L. c-di-
910 GMP regulates type IV pili-dependent-motility in *Myxococcus xanthus*. J Bacteriol 2015;
911 198:77-90.

912 21. Skotnicka D, Smaldone GT, Petters T, Trampari E, Liang J, Kaever V, et al. A minimal
913 threshold of c-di-GMP is essential for fruiting body formation and sporulation in *Myxococcus*
914 *xanthus*. PLOS Genet. 2016; 12:e1006080.

915 22. Petters T, Zhang X, Nesper J, Treuner-Lange A, Gómez-Santos N, Hoppert M, et al.
916 The orphan histidine protein kinase SgmT is a c-di-GMP receptor and regulates composition
917 of the extracellular matrix together with the orphan DNA binding response regulator DigR in
918 *Myxococcus xanthus*. Mol Microbiol. 2012; 84:147-165.

919 23. Kuzmich S, Skotnicka D, Szadkowski D, Klos P, Perez-Burgos M, Schander E, et al.
920 Three PilZ domain proteins, PlpA, PixA and PixB, have distinct functions in regulation of
921 motility and development in *Myxococcus xanthus*. J Bacteriol. 2021; 203:e0012621.

922 24. Kuzmich S, Blumenkamp P, Meier D, Szadkowski D, Goesmann A, Becker A, et al.
923 CRP-like transcriptional regulator MrpC curbs c-di-GMP and 3',3'-cGAMP nucleotide levels
924 during development in *Myxococcus xanthus*. mBio. 2022; 13:e00044-22.

925 25. Treuner-Lange A, Aguiluz K, van der Does C, Gómez-Santos N, Harms A,
926 Schumacher D, et al. PomZ, a ParA-like protein, regulates Z-ring formation and cell division
927 in *Myxococcus xanthus*. Mol Microbiol. 2013; 87:235-53.

928 26. Schumacher D, Bergeler S, Harms A, Vonck J, Huneke-Vogt S, Frey E, et al. The
929 PomXYZ proteins self-organize on the bacterial nucleoid to stimulate cell division. Dev Cell.
930 2017; 41:299-314.

931 27. Lin L, Osorio Valeriano M, Harms A, Søgaard-Andersen L, Thanbichler M. Bactofilin-
932 mediated organization of the ParABS chromosome segregation system in *Myxococcus*
933 *xanthus*. Nat Commun. 2017; 8:1817.

934 28. Bulyha I, Lindow S, Lin L, Bolte K, Wuichet K, Kahnt J, et al. Two small GTPases act
935 in concert with the bactofilin cytoskeleton to regulate dynamic bacterial cell polarity.
936 Developmental cell. 2013; 25:119-131.

937 29. Harms A, Treuner-Lange A, Schumacher D, Søgaard-Andersen L. Tracking of
938 chromosome and replisome dynamics in *Myxococcus xanthus* reveals a novel chromosome
939 arrangement. PLoS Genet. 2013; 9:e1003802.

30. Iniesta AA. ParABS system in chromosome partitioning in the bacterium *Myxococcus xanthus*. PLoS One. 2014; 9:e86897.

31. Jalal ASB, Le TBK. Bacterial chromosome segregation by the ParABS system. Open Biology. 2020; 10:200097.

32. Nolivos S, Sherratt D. The bacterial chromosome: architecture and action of bacterial SMC and SMC-like complexes. FEMS Microbiol Rev. 2014; 38:380-392.

33. Anand D, Schumacher D, Søgaard-Andersen L. SMC and the bactofilin/PadC scaffold have distinct yet redundant functions in chromosome segregation and organization in *Myxococcus xanthus*. Mol Microbiol 2020; 114:839-856.

34. Schreiter ER, Drennan CL. Ribbon-helix-helix transcription factors: variations on a theme. Nat Rev Microbiol. 2007; 5:710-20.

35. Galperin MY, Chou SH. Structural conservation and diversity of PilZ-related domains. J Bacteriol. 2020; 202:e00664-19.

36. Rosario CJ, Singer M. The *Myxococcus xanthus* developmental program can be delayed by inhibition of DNA replication. J Bacteriol. 2007; 189:8793-8800.

37. Corn JE, Berger JM. Regulation of bacterial priming and daughter strand synthesis through helicase-primase interactions. Nucl Acids Res. 2006; 34:4082-4088.

38. Mayer MP. The Hsp70-chaperone machines in bacteria. Frontiers Mol Biosci. 2021; 8:694012.

39. Weimer RM, Creighton C, Stassinopoulos A, Youderian P, Hartzell PL. A chaperone in the HSP70 family controls production of extracellular fibrils in *Myxococcus xanthus*. J Bacteriol. 1998; 180:5357-5368.

40. Mitchell AM, Silhavy TJ. Envelope stress responses: balancing damage repair and toxicity. Nat Rev Microbiol. 2019; 17:417-428.

41. Jurėnas D, Fraikin N, Goormaghtigh F, Van Melderen L. Biology and evolution of bacterial toxin–antitoxin systems. Nat Rev Microbiol. 2022; 20:335-350.

42. LeRoux M, Laub MT. Toxin-antitoxin systems as phage defense elements. Annu Rev Microbiol. 2022; 76:21-43.

43. Casu B, Sallmen JW, Schlimpert S, Pilhofer M. Cytoplasmic contractile injection systems mediate cell death in *Streptomyces*. Nat Microbiol. 2023; 8:711-726.

44. Vladimirov M, Zhang RX, Mak S, Nodwell JR, Davidson AR. A contractile injection system is required for developmentally regulated cell death in *Streptomyces coelicolor*. Nat Commun. 2023; 14:1469.

45. Kimura Y, Nakato H, Ishibashi K, Kobayashi S. A *Myxococcus xanthus* CbpB containing two cAMP-binding domains is involved in temperature and osmotic tolerances. FEMS Microbiol Lett. 2005; 244:75-83.

46. Tzeng L, Singer M. DNA replication during sporulation in *Myxococcus xanthus* fruiting bodies. Proc Natl Acad Sci U S A. 2005; 102:14428-33.

978 47. Janssen GR, Wireman JW, Dworkin M. Effect of temperature on the growth of
979 *Myxococcus xanthus*. J Bacteriol. 1977; 130:561-562.

980 48. Singh A, Izac JR, Schuler EJA, Patel DT, Davies C, Marconi RT. High-resolution
981 crystal structure of the *Borreliella burgdorferi* PlzA protein in complex with c-di-GMP: new
982 insights into the interaction of c-di-GMP with the novel xPilZ domain. Pathog Dis. 2021; 79:1-
983 9.

984 49. Jusufovic N, Savage CR, Saylor TC, Brissette CA, Zückert WR, Schlax PJ, et al.
985 *Borrelia burgdorferi* PlzA is a c-di-GMP dependent DNA and RNA binding protein. bioRxiv.
986 2023:2023.01.30.526351.

987 50. Townsley L, Yildiz FH. Temperature affects c-di-GMP signalling and biofilm formation
988 in *Vibrio cholerae*. Environ Microbiol. 2015; 17:4290-4305.

989 51. Almblad H, Randall TE, Liu F, Leblanc K, Groves RA, Kittichotirat W, et al. Bacterial
990 cyclic diguanylate signaling networks sense temperature. Nat Commun. 2021; 12:1986.

991 52. Kaiser D. Social gliding is correlated with the presence of pili in *Myxococcus xanthus*.
992 Proc Natl Acad Sci U S A. 1979; 76:5952-5956.

993 53. Shi X, Wegener-Feldbrugge S, Huntley S, Hamann N, Hedderich R, Søgaard-
994 Andersen L. Bioinformatics and experimental analysis of proteins of two-component systems
995 in *Myxococcus xanthus*. J Bacteriol. 2008; 190:613-24.

996 54. Hodgkin J, Kaiser D. Cell-to-cell stimulation of movement in nonmotile mutants of
997 *Myxococcus*. Proc Natl Acad Sci U S A. 1977; 74:2938-42.

998 55. Sambrook J, Russell DW. Molecular Cloning: A Laboratory Manual. 3rd ed. Cold
999 Spring Harbor, N.Y.: Cold Spring Harbor Laboratory Press; 2001.

1000 56. Søgaard-Andersen L, Slack FJ, Kimsey H, Kaiser D. Intercellular C-signaling in
1001 *Myxococcus xanthus* involves a branched signal transduction pathway. Genes Dev. 1996;
1002 10:740-754.

1003 57. Bulyha I, Schmidt C, Lenz P, Jakovljevic V, Höne A, Maier B, et al. Regulation of the
1004 type IV pili molecular machine by dynamic localization of two motor proteins. Mol Microbiol
1005 2009; 74:691–706.

1006 58. Schindelin J, Arganda-Carreras I, Frise E, Kaynig V, Longair M, Pietzsch T, et al. Fiji:
1007 an open-source platform for biological-image analysis. Nat Methods. 2012; 9:676-82.

1008 59. Herfurth M, Treuner-Lange A, Glatter T, Wittmaack N, Hoiczyk E, Pierik AJ, et al. A
1009 noncanonical cytochrome c stimulates calcium binding by PilY1 for type IVa pili formation.
1010 Proc Natl Acad Sci U S A. 2022; 119.

1011 60. Schmittgen TD, Livak KJ. Analyzing real-time PCR data by the comparative C(T)
1012 method. Nat Protoc. 2008; 3:1101-8.

1013 61. Paintdakhi A, Parry B, Campos M, Irnov I, Elf J, Surovtsev I, et al. Oufti: an integrated
1014 software package for high-accuracy, high-throughput quantitative microscopy analysis. Mol
1015 Microbiol. 2016; 99:767-77.

62. Fernández-Coll L, Maciag-Dorszynska M, Tailor K, Vadia S, Levin PA, Szalewska-Palasz A, et al. The absence of (p)ppGpp renders initiation of *Escherichia coli* chromosomal DNA synthesis independent of growth rates. mBio. 2020; 11:e03223-19

63. Gómez-Santos N, Glatter T, Koebnik R, Świątek-Połatyńska MA, Søgaard-Andersen L. A TonB-dependent transporter is required for secretion of protease PopC across the bacterial outer membrane. Nat Commun. 2019; 10:1360.

64. Cox J, Mann M. MaxQuant enables high peptide identification rates, individualized p.p.b.-range mass accuracies and proteome-wide protein quantification. Nat Biotechnol. 2008; 26:1367-1372.

65. Schwanhäusser B, Busse D, Li N, Dittmar G, Schuchhardt J, Wolf J, et al. Global quantification of mammalian gene expression control. Nature. 2011; 473:337-342.

66. Tyanova S, Temu T, Sinitcyn P, Carlson A, Hein MY, Geiger T, et al. The Perseus computational platform for comprehensive analysis of (prote)omics data. Nat Methods. 2016; 13:731-740.

67. Perez-Riverol Y, Bai J, Bandla C, García-Seisdedos D, Hewapathirana S, Kamatchinathan S, et al. The PRIDE database resources in 2022: a hub for mass spectrometry-based proteomics evidences. Nucl Acids Res. 2021; 50:D543-D552.

68. Jumper J, Evans R, Pritzel A, Green T, Figurnov M, Ronneberger O, et al. Highly accurate protein structure prediction with AlphaFold. Nature. 2021; 596:583-589.

69. Mirdita M, Schütze K, Moriwaki Y, Heo L, Ovchinnikov S, Steinegger M. ColabFold: making protein folding accessible to all. Nat Methods. 2022; 19:679-682.

70. Potter SC, Luciani A, Eddy SR, Park Y, Lopez R, Finn RD. HMMER web server: 2018 update. Nucl Acids Res. 2018; 46:W200-W204.

71. Kumar S, Stecher G, Li M, Knyaz C, Tamura K. MEGA X: Molecular evolutionary genetics analysis across computing platforms. Mol Biol Evol. 2018; 35:1547-1549.

72. Li W, Cowley A, Uludag M, Gur T, McWilliam H, Squizzato S, et al. The EMBL-EBI bioinformatics web and programmatic tools framework. Nucl Acids Res. 2015; 43:W580-4.

73. Julien B, Kaiser AD, Garza A. Spatial control of cell differentiation in *Myxococcus xanthus*. Proc Natl Acad Sci U S A. 2000; 97:9098-103.

74. Jakovljevic V, Leonardy S, Hoppert M, Søgaard-Andersen L. PilB and PilT are ATPases acting antagonistically in type IV pilus function in *Myxococcus xanthus*. J Bacteriol. 2008; 190:2411-21.

75. Wu SS, Kaiser D. Genetic and functional evidence that Type IV pili are required for social gliding motility in *Myxococcus xanthus*. Mol Microbiol. 1995; 18:547-58.

76. Wu SS, Kaiser D. Regulation of expression of the *pilA* gene in *Myxococcus xanthus*. J Bacteriol. 1997; 179:7748-7758.

77. Treuner-Lange A, Chang Y-W, Glatter T, Herfurth M, Lindow S, Chreifi G, et al. PilY1 and minor pilins form a complex priming the type IVa pilus in *Myxococcus xanthus*. Nat Commun. 2020; 11:5054.

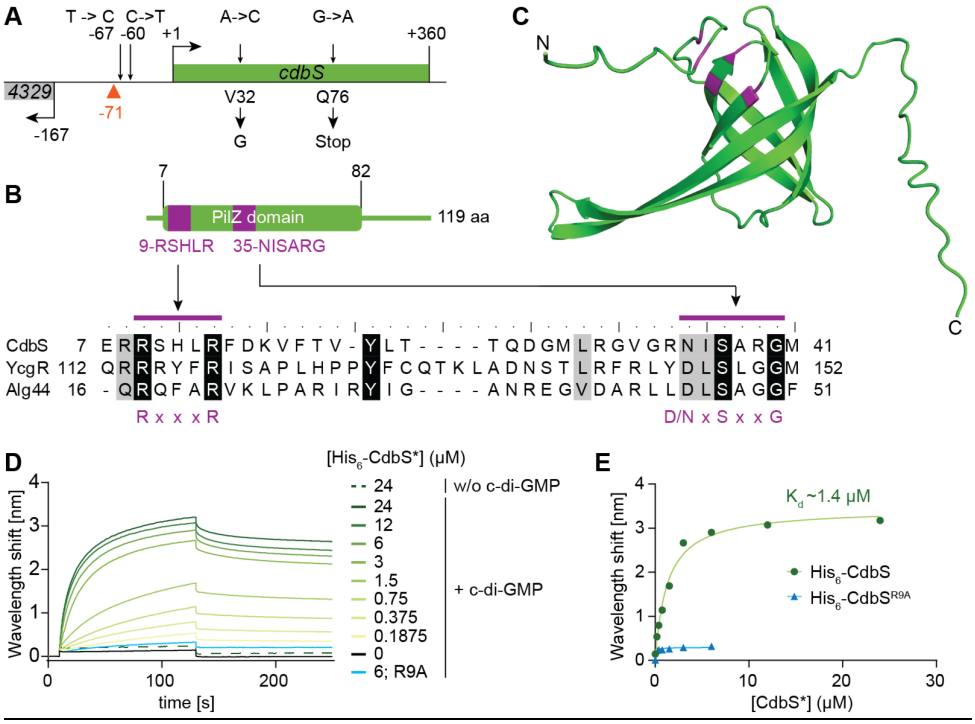

Fig. 1. CdbS is a stand-alone PilZ domain protein and binds c-di-GMP

A. *cdbS* locus. Kinked arrows indicate transcription start sites and +1 the transcription start site of *cdbS* [24]. Suppressor mutations upstream of and within *cdbS* are indicated by arrows above and amino acid substitutions/stop codon below. The red triangle indicates the CdbA peak summit at -71 from a ChIP-seq analysis in which an active CdbA-FLAG protein was used as bait [11]. **B.** CdbS is a stand-alone PilZ domain protein. The PilZ domain encompasses residues 7-82. The residues marked in purple indicate the bipartite c-di-GMP binding motif. Below, alignment of residues 7-41 of CdbS with the corresponding residues of the PilZ domains of *E. coli* YcgR [6] and *P. aeruginosa* Alg44 [5]. Residues marked with purple bars indicate the bipartite c-di-GMP binding motif with the consensus below [2]. **C.** AlphaFold model of CdbS. CdbS was modeled as a monomer. Model rank 1 is shown with the conserved residues in the bipartite c-di-GMP binding motif marked in purple. **D.** Bio-layer interferometric analysis of the interaction between CdbS variants and c-di-GMP. Streptavidin coated sensors were loaded with biotinylated c-di-GMP and probed with the indicated concentrations of His_6-CdbS (shades of green) or His_6-$CdbS^{R9A}$ (blue). The interaction kinetics were followed by monitoring the wavelength shifts resulting from changes in the optical thickness of the sensor surface during association or dissociation of the analyte. Unspecific binding of His_6-CdbS to the sensor was tested in the absence of c-di-GMP (w/o c-di-GMP) and is shown as the dashed line. **E.** Analysis of the binding data shown in panel D. Plot shows the equilibrium levels measured at the indicated His_6-CdbS* concentrations. The data were fitted to a non-cooperative one-site specific-binding model. The calculated K_d for His_6-CdbS is shown in the graph.

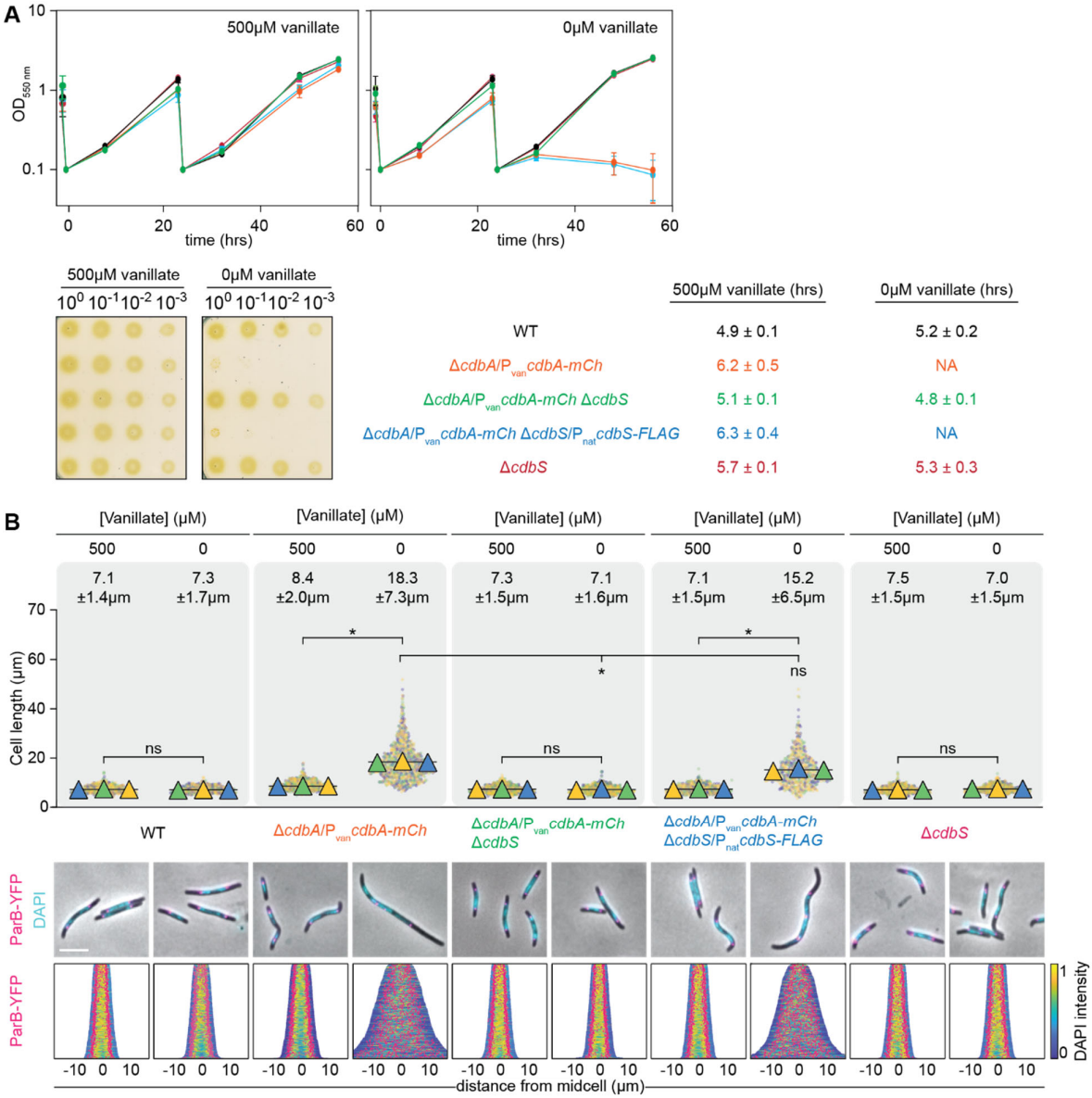

Figure 2: Lack of CdbS suppresses CdbA essentiality

A. Growth of strains of indicated genotypes. Cells were grown in 1% CTT broth in suspension culture (upper) or on 1% CTT broth, 1.5% agar on a solid surface (lower) in the presence and absence of vanillate as indicated. Plates were incubated for 96hrs before imaging. Color code used for the growth curves are as in the table. Table indicates generation times as mean ± standard deviation (STDEV) from three biological replicates; NA, not applicable. **B.** Cell length and chromosome organization of strains of indicated genotypes. Cells were grown in the presence and absence of vanillate as indicated. In the absence of vanillate, cells were analyzed 24hrs after removal of vanillate. Cell length measurements are included from three independent experiments indicated in different colored triangles and the mean is based on all three experiments. Numbers above indicate cell length as mean ± STDEV from all three experiments. * *P*<0.0001, ns, not significant in 2way ANOVA multiple comparisons test. Total number of cells analyzed: 440-870. Lower diagrams, fluorescence microscopy images of cells stained with DAPI and synthesizing

ParB-YFP. In the demographs, cells are sorted according to length, DAPI signals are shown according to the intensity scale, and ParB-YFP signals in pink. Scale bar, 5μm. N=400 cells for all strains. In A and B, all strains are *parB*$^{+}$/*parB-YFP* merodiploid.

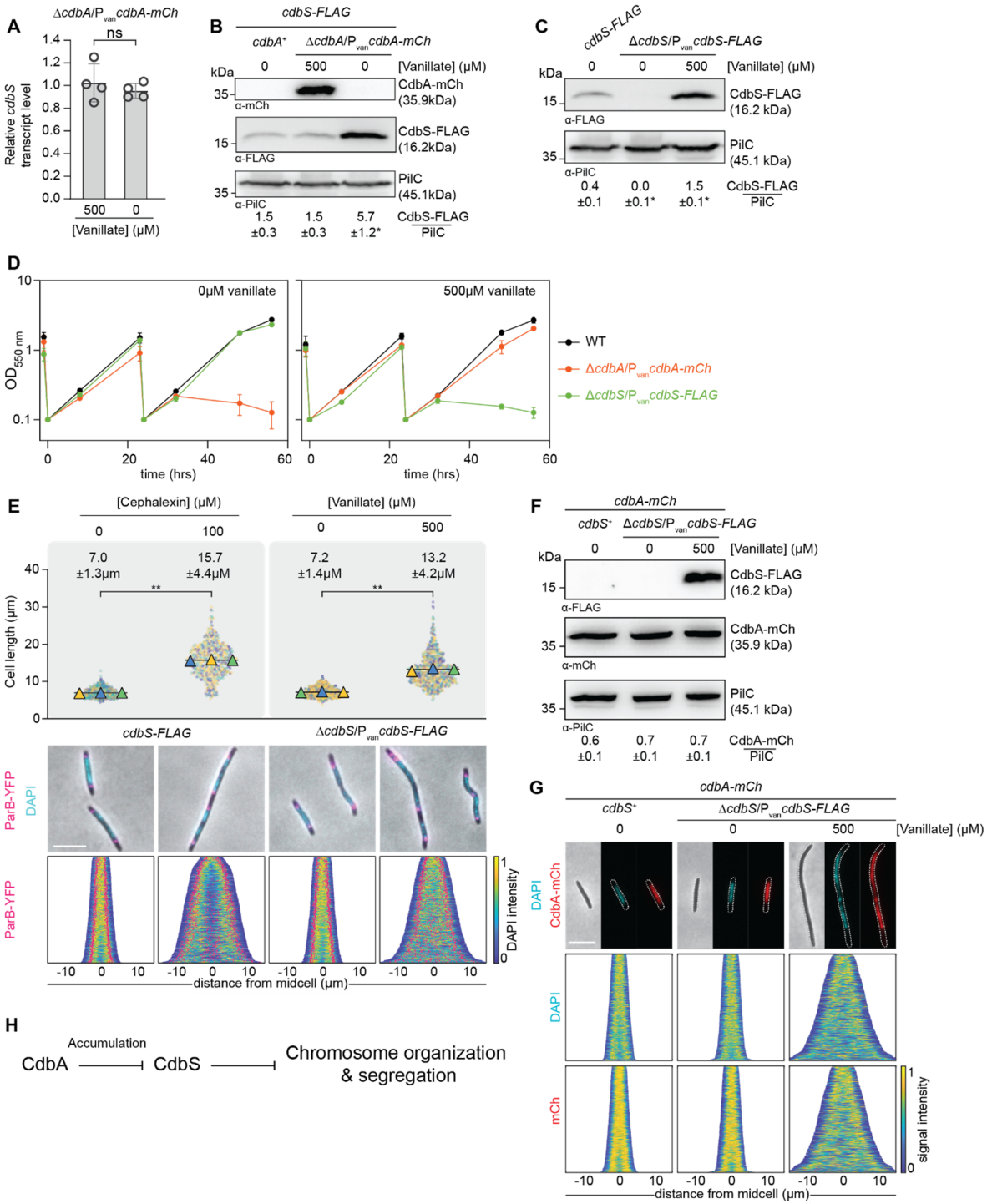

Figure 3. Overexpression of *cdbS* phenocopies CdbA-depletion

A. RT-qPCR analysis of *cdbS* expression in the presence and absence of CdbA-mCh. Cells of the indicated genotypes were grown in the presence of vanillate or in its the absence for 24hrs. Transcript levels are shown relative to the level in the presence of vanillate and as mean ± STDEV from four biological replicates with three technical replicates each. Individual data points are shown in black. ns, no significant difference in two-sided Student's t-test. **B.** Immunoblot analysis of CdbS-FLAG accumulation in the presence and absence of CdbA-

mCh. Cells of the indicated genotypes were grown in the presence or absence of vanillate as in A. The same amount of total protein was loaded per lane. PilC is used as a loading control. Numbers below show the mean level of CdbS-FLAG normalized by the PilC level ± STDEV calculated from three independent experiments. *, $P<0.05$ in Student's t test in which samples were compared to the *cdbA*$^+$ strain. **C.** Immunoblot analysis of CdbS-FLAG accumulation. Cells of the indicated genotypes were grown in the absence of vanillate or in its presence for 24hrs. The *cdbS-FLAG* strain expresses this allele from the native site. Samples were loaded and analyzed as in B. *, $P<0.05$ in Student's t test in which samples were compared to CdbS-FLAG expressed from the native site. **D.** Growth of strains of indicated genotypes. Cells were grown in 1% CTT broth in suspension culture in the presence and absence of vanillate as indicated. The growth curves were prepared from three biological replicates, error bars, mean ± STDEV.
E. Cell length and chromosome organization of strains of indicated genotypes. Cells were grown as in C. Cells grown in the presence of cephalexin were analyzed after 8hrs. Cells were analyzed as in Fig 2B. Numbers above indicate cell length as mean ± STDEV from all three experiments. **, $P<0.0001$, ns, not significant in 2way ANOVA multiple comparisons test. Total number of cells analyzed: 497-794. Lower panels, scale bar, 5μm. N = 400 cells for all strains. **F.** Immunoblot analysis of CdbA-mCh accumulation in strains with varying CdbS levels. Cells were grown as in C and samples loaded and analyzed as in B based on three biological replicates. **G.** Phase contrast and fluorescence microscopy images of cells of the indicated genotypes stained with DAPI and expressing CdbA-mCh. Cells were grown as in C. In the demographs, cells are sorted by cell length, DAPI and mCh signals are shown according to the intensity scale. Scale bar, 5μm. N=400 cells for all strains. **H.** Genetic pathway for the CdbA CdbS interaction. See text for details. In A-G, all strains are *parB*$^+$/*parB-YFP* merodiploid.

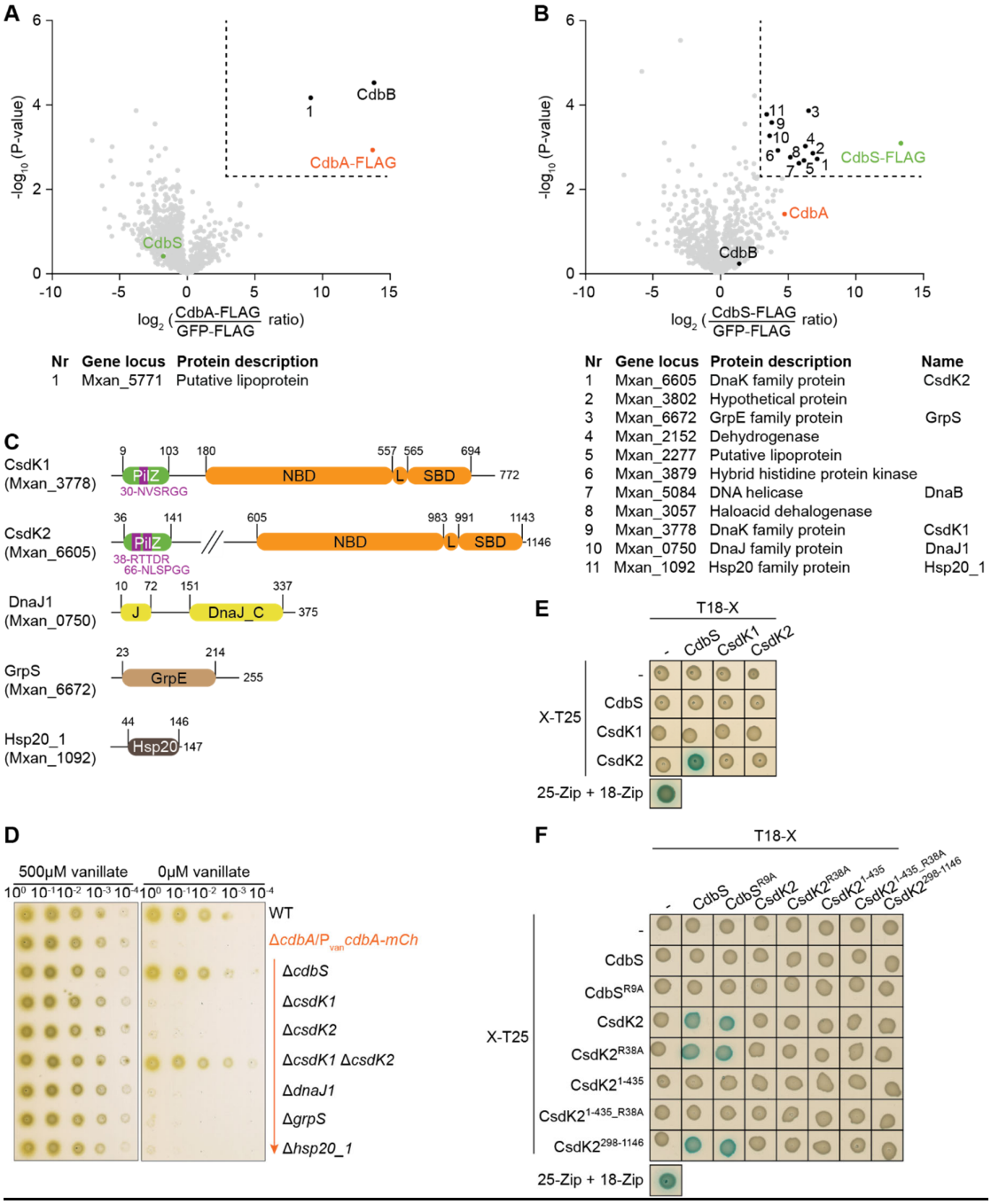

Nr	Gene locus	Protein description
1	Mxan_5771	Putative lipoprotein

Nr	Gene locus	Protein description	Name
1	Mxan_6605	DnaK family protein	CsdK2
2	Mxan_3802	Hypothetical protein	
3	Mxan_6672	GrpE family protein	GrpS
4	Mxan_2152	Dehydrogenase	
5	Mxan_2277	Putative lipoprotein	
6	Mxan_3879	Hybrid histidine protein kinase	
7	Mxan_5084	DNA helicase	DnaB
8	Mxan_3057	Haloacid dehalogenase	
9	Mxan_3778	DnaK family protein	CsdK1
10	Mxan_0750	DnaJ family protein	DnaJ1
11	Mxan_1092	Hsp20 family protein	Hsp20_1

Figure 4. CdbS interacts with two PilZ-DnaK proteins

A, B. Volcano plot visualizing potential interaction candidates of CdbA-FLAG (A) and CdbS-FLAG (B). *In vivo* pull-down using CdbA-FLAG or CdbS-FLAG as bait compared to GFP-FLAG (negative control). Samples from four biological replicates were analyzed by label-free mass spectrometry-based quantitative proteomics, and mean iBAQ values and log2-fold enrichment in experimental samples compared to GFP-FLAG samples calculated. X-axis, log2-fold enrichment of proteins with the indicated bait protein versus the control sample expressing GFP-FLAG. Y-axis, -log10 of *P*-value. Significantly enriched proteins in the experimental samples (log2 ratio ≥3; *P*-value ≤0.005 (-log10 ≥2.3) are indicated by the

stippled lines. Enriched proteins are indicated or numbered and explained in the tables below. **C.** Domain architecture of chaperones and co-chaperones enriched in the pull-down experiments with CdbS-FLAG. In CsdK1 and CsdK2, residues in purple indicate the c-di-GMP binding motifs (see also Fig 1B), NBD the nucleotide binding domain, L the conserved linker, and SBD the substrate binding domain. **D.** Cells lacking CsdK1 as well as CsdK2 and depleted of CdbA-mCh are viable. Cells were grown on 1% CTT broth, 1.5% agar on a solid surface in the presence and absence of vanillate as indicated. Plates were incubated for 96hrs before imaging. Similar results were observed in three independent experiments. All strains are Δ*cdbA*/P_{van}*cdbA-mCh* and *parB*$^{+}$/*parB-YFP* merodiploid. **E.** BACTH analysis of CdbS and CsdK1 and CsdK2 interactions. The indicated full-length proteins were fused to the N-terminus of T25 or the C-terminus of T18 as indicated. Blue and white colony colors indicate an interaction and no interaction, respectively. T25-Zip + T18-Zip, positive control; the strains in the row and column labelled "–" contain the indicated plasmid and an empty plasmid and served as controls for self-activation. The same results were observed in two biological replicates. **F.** BACTH analysis of CdbS and CsdK2 interaction. The indicated protein variants were fused to the N-terminus of T25 or the C-terminus of T18 as indicated. Controls as in E. The same results were observed in two biological replicates.

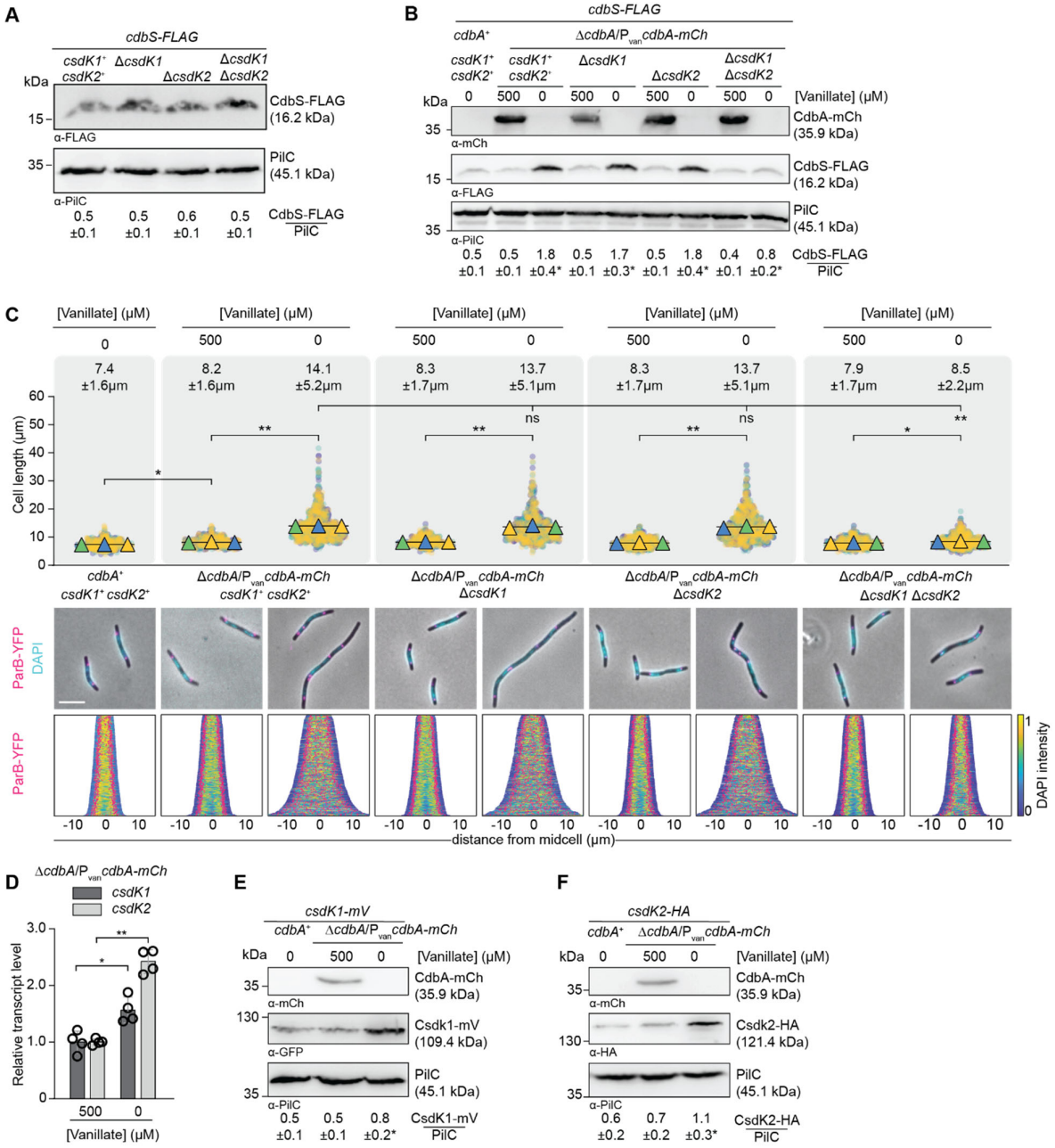

Figure 5. CsdK1 and CsdK2 jointly stabilize CdbS during CdbA depletion

A. Immunoblot analysis of CdbS-FLAG accumulation in strains lacking CsdK1, CsdK2 or both. Samples were loaded and analyzed as in Fig 3B based on three biological replicates. In Student's t test in which samples were compared to the *csdK1*$^+$ *csdK2*$^+$ strain, no significant differences were observed. *cdbS-FLAG* is expressed from the native site. **B.** Immunoblot analysis of CdbS-FLAG accumulation in strains lacking CsdK1, CsdK2 or both and depleted of CdbA-mCh. Cells of the indicated genotypes were grown in the presence of vanillate or in its absence for 24hrs. *cdbS-FLAG* is expressed from the native site. Samples were loaded and analyzed as in Fig 3B based on three biological replicates. *, *P*<0.05 in Student's t test in which samples are compared to the *cdbA*$^+$ strain. **C.** Cell length and chromosome organization of strains of indicated genotypes. Cells were grown as in B. Cells were analyzed as in Fig 2B. Numbers above indicate cell length as mean ± STDEV from all

three experiments. *, $P<0.001$, ** $P<0.0001$, and ns, not significant in 2way ANOVA multiple comparisons test. Total number of cells analyzed: 544-923. Lower diagrams, scale bar, 5µm. N=400 cells for all strains. **D.** RT-qPCR analysis of *csdK1* and *csdK2* transcript levels in the presence and absence of CdbA-mCh. Cells of the indicated genotypes were grown as in B. Transcript levels are indicated relative to the level in the presence of 500µM vanillate as mean ± STDEV from four biological replicates with three technical replicates each. *, $P<0.01$, **, $P<0.0001$ in two-sided Student's t-test. **E, F.** Immunoblot analysis of CsdK1-mV (E) and CsdK2-HA (F) accumulation in the presence and absence of CdbA-mCh. Cells were grown as in B. Samples were loaded and analyzed as in Fig 3B based on three biological replicates. *, $P<0.05$ in Student's t test in which samples were compared to the *cdbA*$^+$ strain. In A-D, all strains are *parB*$^+$/*parB-YFP* merodiploid.

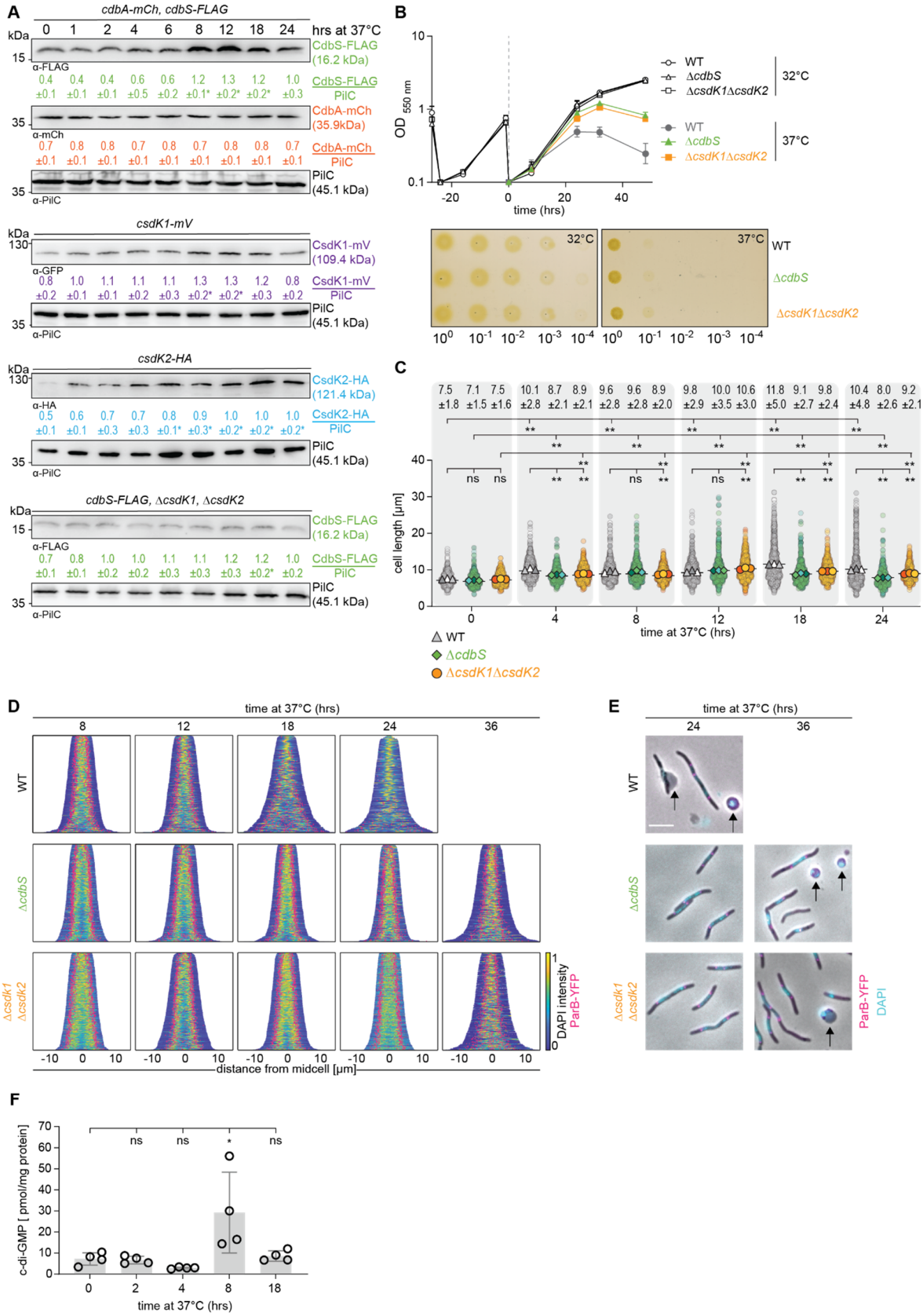

Figure 6. CdbS accumulates at an increased level at 37°C and accelerates cell death

A. Immunoblot analysis of CdbS-FLAG, CdbA-mCh, CsdK1-mV and CsdK2-HA accumulation at 37°C. Cells of the indicated genotypes were grown at 32°C and shifted to 37°C at t=0hrs. All strains express the relevant protein from the native site. CdbS-FLAG and CdbA-mCh were synthesized in the same strain. Samples were loaded and anylzed as in Fig 3 based on three biological replicates. *, $P<0.05$ in Student's t test in which samples were compared to protein levels at t=0hrs. **B.** Growth of strains of indicated genotypes. Cells were grown in 1% CTT broth in suspension culture (upper) or on 1% CTT broth, 1.5% agar on a solid surface (lower) at 32°C and 37°C as indicated. Growth curves were generated from three independent experiments. Plates were incubated for 96hrs before imaging and similar results were obtained in three biological replicates. **C, D.** Cell length analyses and chromosomes organization in strains of the indicated genotypes during growth at 37°C. Cells were grown at 37°C as indicated. In C, cells were analyzed as in Fig 2B. Only rod-shaped cells were included in the measurements. Numbers above indicate cell length as mean ± STDEV calculated from three biological replicates. Total number of cells analyzed: 487-770. *, $P<0.01$, **, $P<0.0001$, ns, not significant in 2way ANOVA multiple comparisons test. In D, only rod-shaped cells were included in the analysis and not cell that were undergoing lysis or had rounded up (See E) and cells are sorted according to length, DAPI signals are shown according to the intensity scale, and ParB-YFP signals in pink. N=400 cells for all strains. **E.** Microscopic analysis of cells of the indicated genotypes at 37°C for the indicated periods. Cells were stained with DAPI (blue signal) and synthesizing ParB-YFP (pink signal). Arrows point to cells undergoing lysis or cells that have lost their rod-shape and have rounded up. Scale bar, 5μm. **F.** c-di-GMP level during growth at 37°C. Cells were harvested at the indicated time points of incubation at 37°C, and c-di-GMP levels and protein concentrations determined. Levels are shown as mean ± STDEV calculated from four biological replicates. Individual data points are in black. *, $P<0.05$ in Student's t test. In B-F, all strains are *parB*$^{+}$/*parB-YFP* merodiploid.

Supplementary Figures and Tables

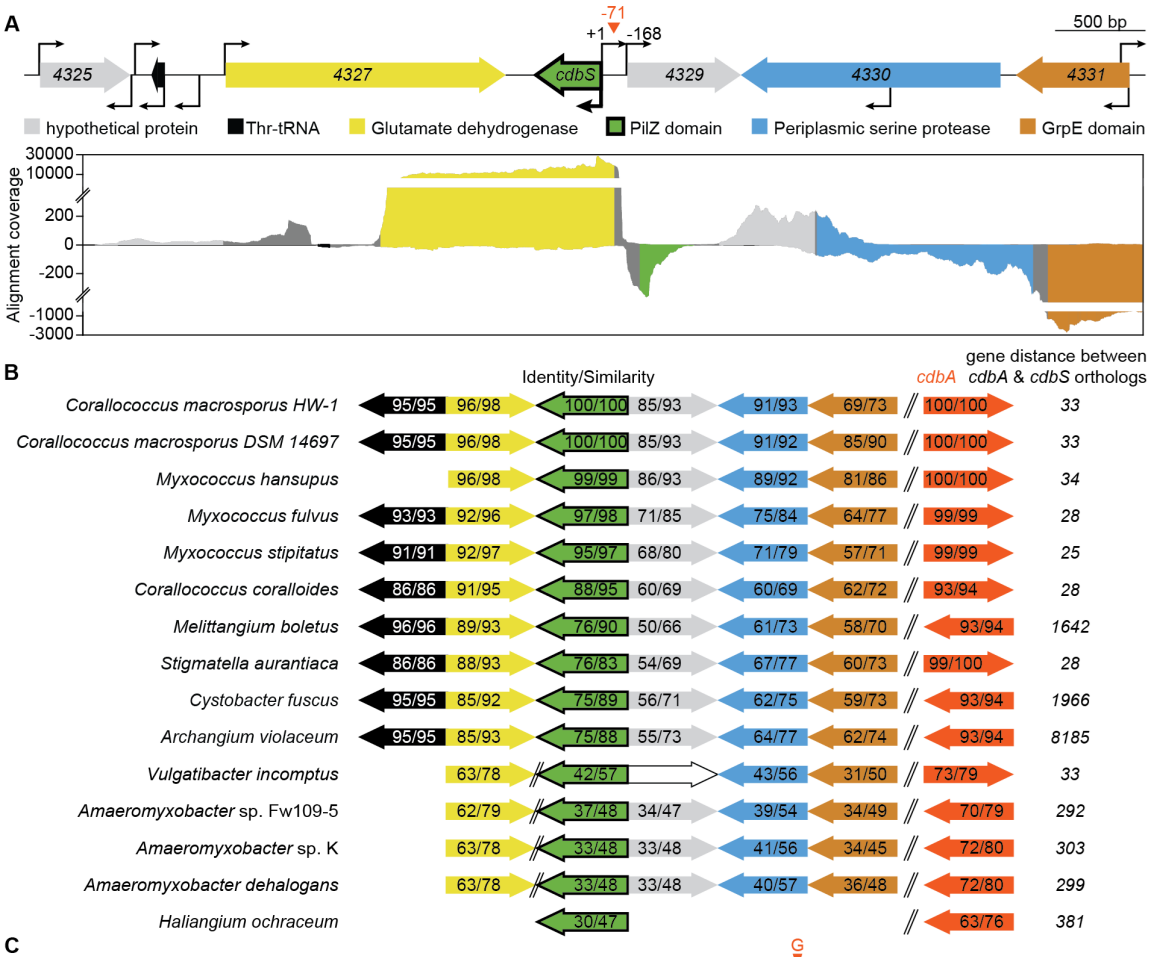

S1 Fig. Analysis of the *cdbS* locus and the CdbS protein.

A. *cdbS* locus. Upper diagram, transcription direction is indicated by the orientation of arrows, kinked arrows indicate transcription start sites as mapped in [24]. Coordinates indicate bp relative to the transcription start site of *cdbS*. Red triangle indicates the CdbA

peak summit from a ChIP-seq analysis in which an active CdbA-FLAG protein was used as bait [11]. The lower diagram show data from RNAseq as base-by-base alignment coverage for total RNA isolated from cells growing in 1% CTT broth [24]. Positive and negative values indicate reads mapped to the forward and reverse strand, respectively. Reads assigned to a gene are colored according to the gene color code in the upper diagram; intergenic regions are in gray. Numbers in genes show mxan_ locus-tags. **B.** The *cdbS* locus is conserved in myxobacteria. Transcription direction is indicated by the orientation of arrows with the color used in A. CdbS homologs were identified using reciprocal BLASTP analysis. Numbers indicated % similarity/identity between CdbS of *M. xanthus* and homologs. % similarity/identity were calculated using EMBOSS Needle software (pairwise sequence alignment). **C.** Alignment of CdbS proteins. Proteins were aligned with default parameters in MEGA7. Amino acid substitution/stop codon caused by *cdbS* suppressor mutations are indicated in red.

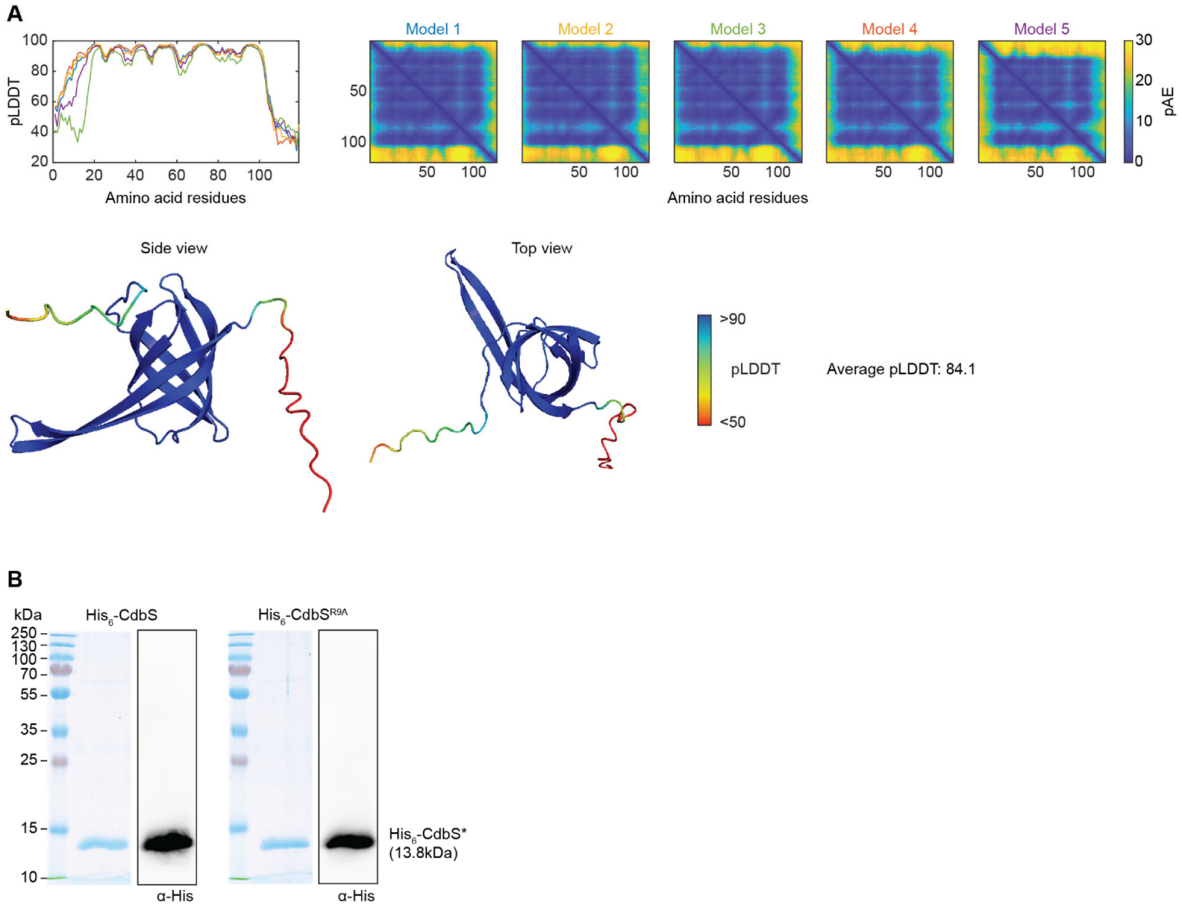

S2 Fig. AlphaFold model of CdbS.

A. pLDDT (Predicted Local Distance Difference Test) and pAE (predicted Alignment Error) plots for five models of CdbS (A) as predicted by AlphaFold. Model rank 1 was used for further analysis and is shown below colored based on pLDDT. **B.** SDS-PAGE analysis of purified His_6-CdbS proteins used *in vitro*. 1µg of the indicated purified proteins were separated by SDS-PAGE and gels stained with InstantBlue and corresponding immunoblot analysis with α-His6 antibodies.

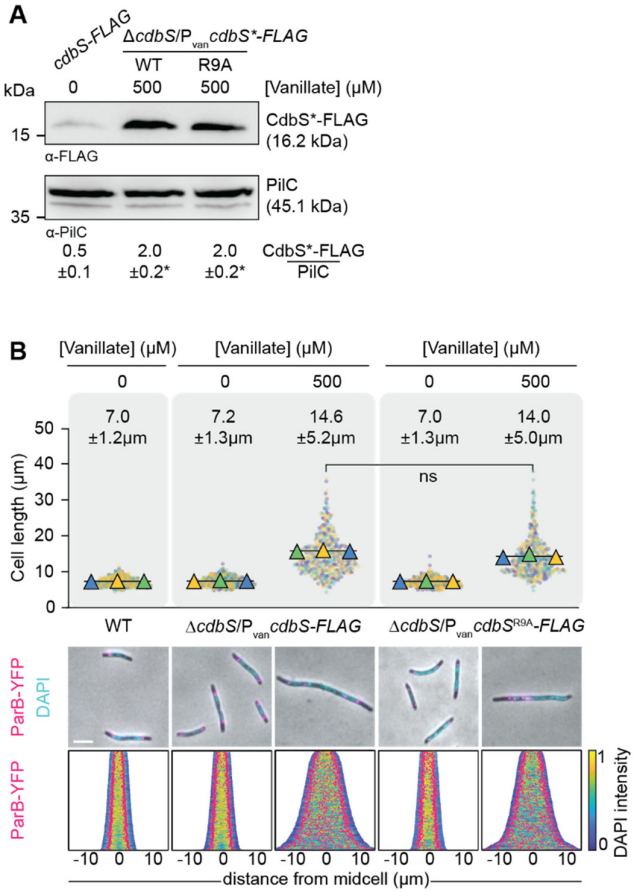

S3 Fig. c-di-GMP binding by CdbS is not important for its activity *in vivo*.

A. Immunoblot analysis of CdbS*-FLAG accumulation. Cells of the indicated genotypes were grown in the presence or absence of the indicated concentrations of vanillate. Cells grown in the presence of vanillate were analyzed 24hrs after addition of vanillate. The *cdbS-FLAG* strain expresses this allele from the native site. The same amount of total protein was loaded per lane. PilC is used as a loading control. Numbers below show the mean ± STDEV of CdbS-FLAG normalized by the PilC level calculated from three independent experiments. *, $P<0.05$ in Student's t test in which samples were compared to CdbS-FLAG expressed from the native site. All strains are *parB*$^+$/*parB-YFP* merodiploid. **B.** Cell length and chromosome organization of strains of indicated genotypes. Cells were grown in 1% CTT broth in the presence and absence of vanillate as indicated. Cells grown in the presence of vanillate were analyzed 24hrs after addition of vanillate. Cell length measurements are included from three independent experiments indicated in different colored triangles and the mean based on all three experiments. Numbers above indicate cell length as mean ± STDEV from all three experiments. ns, not significant in 2way ANOVA multiple comparisons test. Total number of cells analyzed: 469-643. Lower panels, fluorescence microscopy images of cells stained with DAPI and synthesizing ParB-YFP. In the demographs, cells are sorted according to length, DAPI signals are shown according to the intensity scale, and ParB-YFP signals in pink. Scale bar, 5μm. N = 400 cells for all strains. All strains are *parB*$^+$/*parB-YFP* merodiploid.

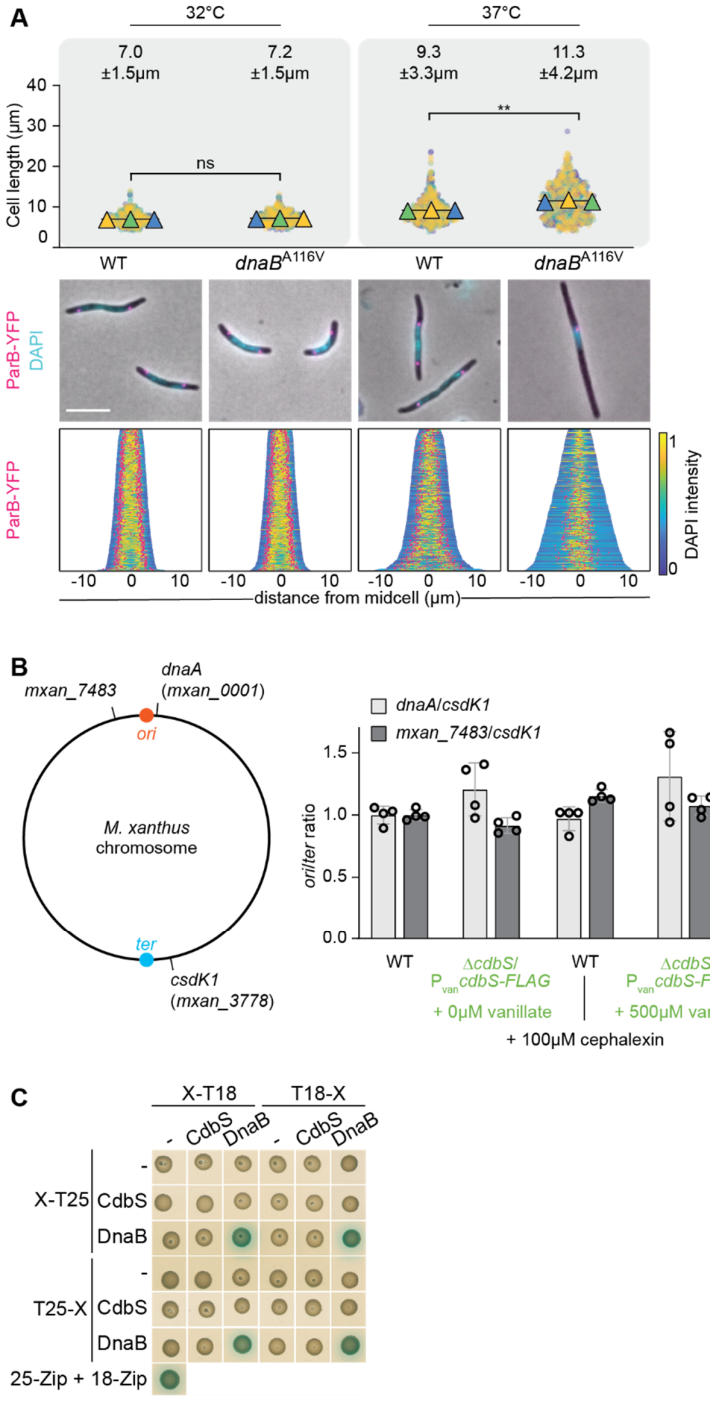

S4 Fig. High CdbS levels do not affect DNA replication.

A. Cell length and chromosome organization of strains of indicated genotypes. Cells were grown at 37°C for 12hrs before the analysis. Cell length measurements are from three independent experiments indicated in different colored triangles and the mean is based on all three experiments. Numbers above indicate cell length as mean ± STDEV from all three experiments. ** *P*<0.0001, ns, not significant in 2way ANOVA multiple comparisons test. Total number of cells analyzed: 603-769. Lower diagrams, fluorescence microscopy images of cells stained with DAPI and synthesizing ParB-YFP. In the demographs, cells are sorted

according to length, DAPI signals are shown according to the intensity scale, and ParB-YFP signals in pink. Scale bar, 5μm. N=400 cells for all strains. All strains are *parB*$^{+}$/*parB-YFP* merodiploid. **B.** qPCR analysis of *ori*/*ter* ratio in indicated strains. Left diagram, the positions on the *M. xanthus* chromosome of the primers used for determination of the *ori/ter* ratio. Right diagram, ratios are shown relative to the level in untreated WT as mean ± STDEV from four biological replicates with three technical replicates each. In pairwise comparisons, no significant differences were observed in 2way ANOVA multiple comparisons test. Both strains are *parB*$^{+}$/*parB-YFP* merodiploid. **C.** BACTH analysis of CdbS and DnaB interaction. The indicated proteins were fused to the N-terminus and C-terminus of T25 or the N- and C-terminus of T18 as indicated. Blue and white colony colours indicate an interaction and no interaction, respectively. T25-Zip + T18-Zip, positive control; the strains in the row and column labelled "–" contain the indicated plasmid and an empty plasmid and served as controls for self-activation. The same results were observed in two biological replicates.

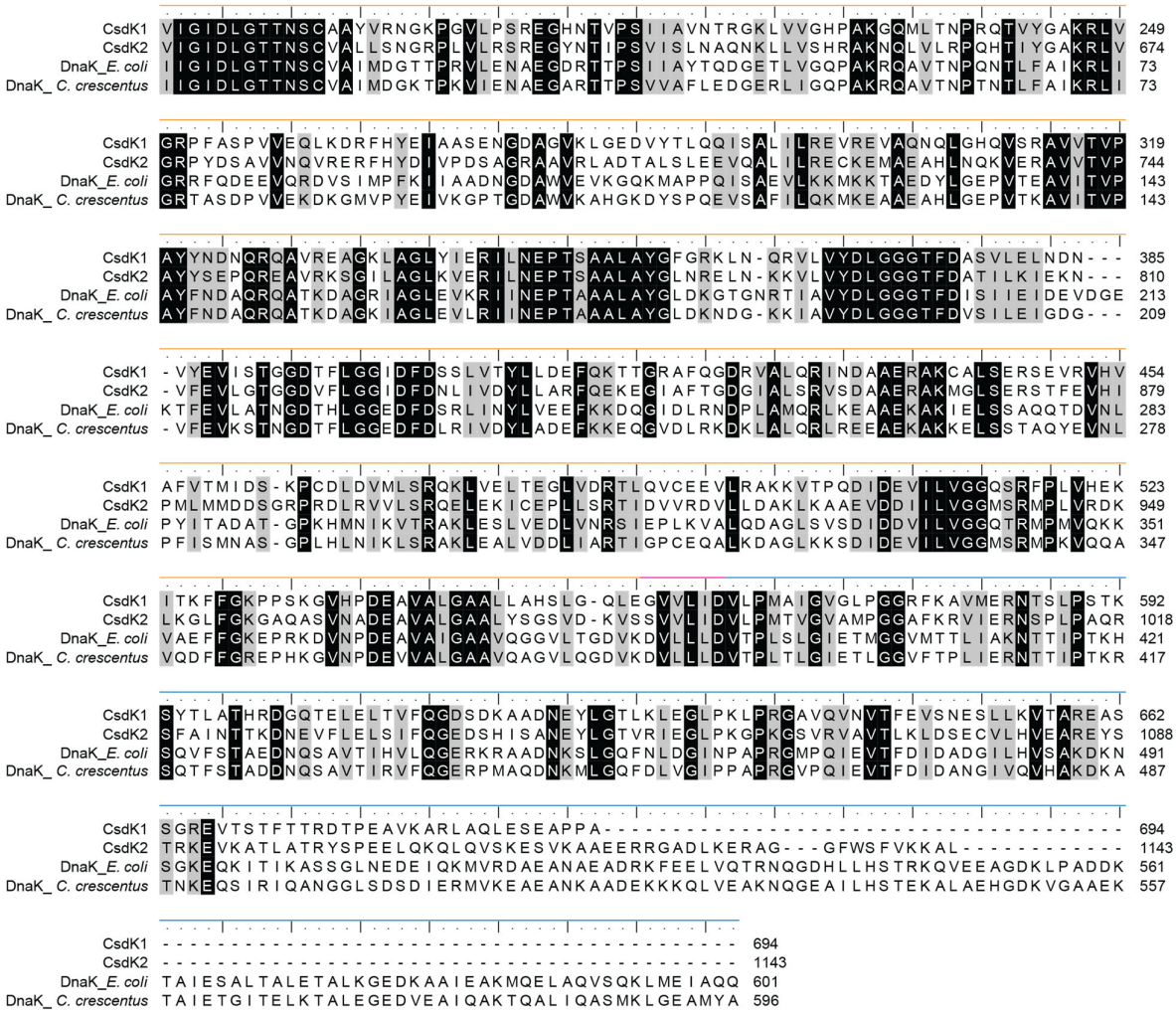

S5 Fig. Sequence analysis of CsdK1 and CsdK2.

Alignment of the DnaK characteristic domains of CsdK1 and CsdK2 with those of DnaK proteins of *E. coli* and *C. crescentus*. The nucleotide-binding domain (orange), the linker (pink) and the substrate-binding domain (blue) are indicated.

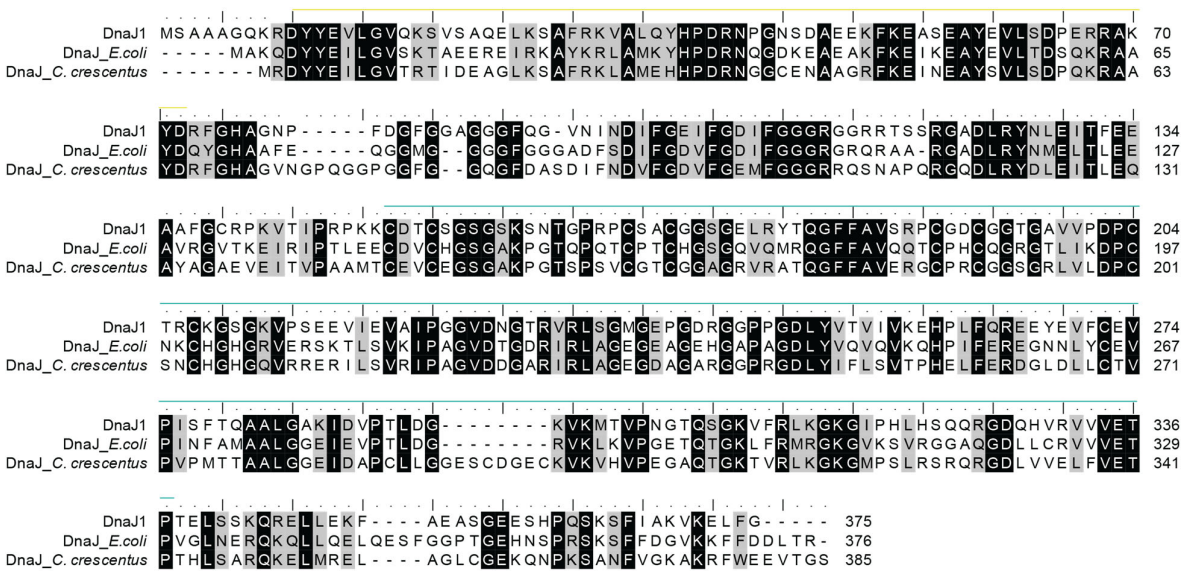

S6 Fig. Sequence analysis of DnaJ1.

Alignment of full-length DnaJ1 with DnaJ of *E. coli* and *C. crescentus*. The J domain (yellow) and the J_central domain (turquoise) are indicated.

S7 Fig. Sequence analysis of GrpS.

Alignment of the GrpE domain of GrpS with those of GrpE of *E. coli* and *C. crescentus*. The GrpE domain (brown) is indicated.

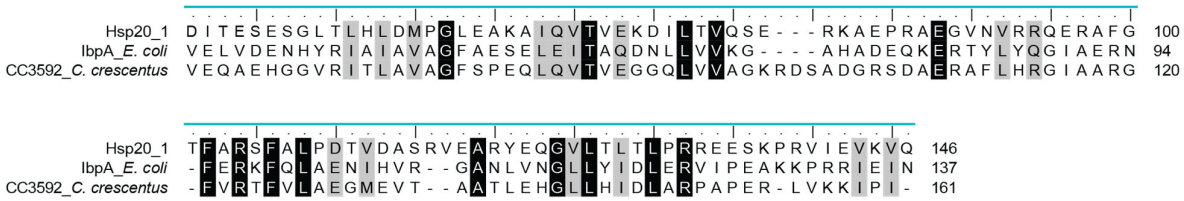

S8 Fig. Sequence analysis of Hsp20_1.

Alignment of the Hsp20 domain of Hsp20_1 with those of IbpA of *E. coli* and the domain of CC_3592 of *C. crescentus*. The Hsp20 domain (cyan) is indicated.

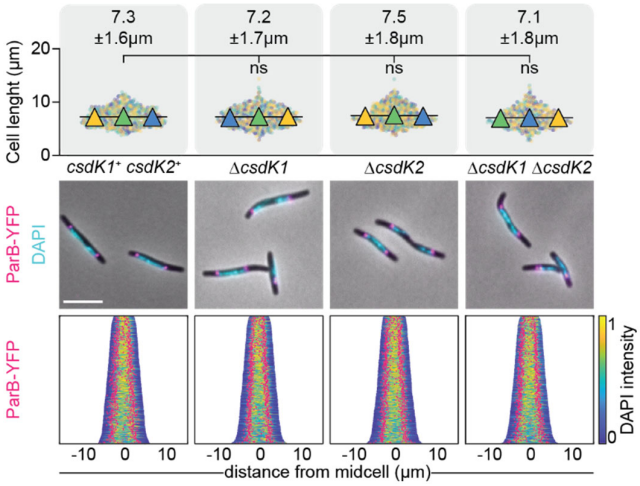

S9 Fig. Lack of CsdK1 and CsdK2 do not affect cell length and chromosome organization. Cell length and chromosome organization of strains of indicated genotypes. Cell length measurements are included from three independent experiments indicated in different colored triangles and the mean calculated based on all three experiments. Numbers above indicate cell length as mean ± STDEV from all three experiments. ns, not significant in 2way ANOVA multiple comparisons test. Total number of cells analyzed: 540-719. Lower diagrams, fluorescence microscopy images of cells stained with DAPI and expressing ParB-YFP. In the demographs, cells are sorted according to length, DAPI signals are shown according to the intensity scale, and ParB-YFP signals in pink. Scale bar, 5μm. N=400 cells for all strains. All strains are *parB*$^{+}$/*parB-YFP* merodiploid.

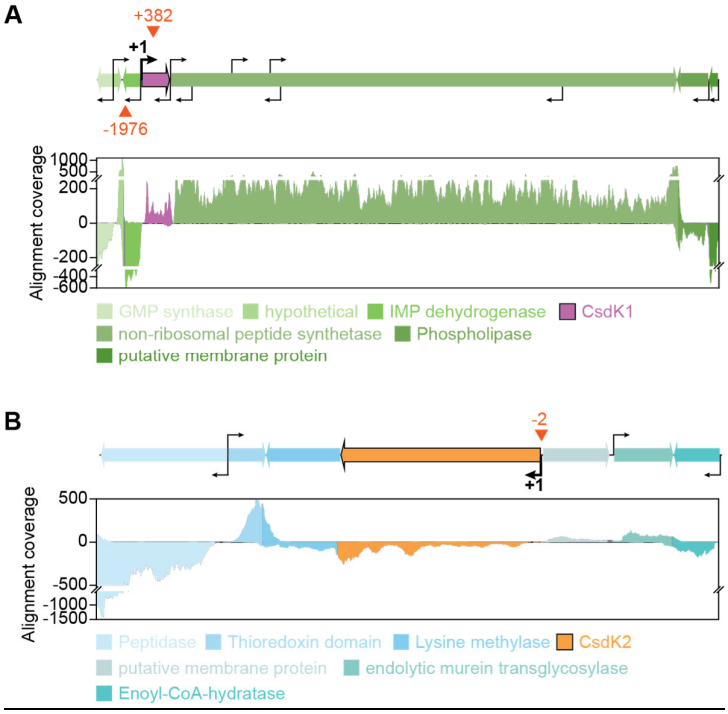

S10 Fig. Organization of the *csdK1* (A) and *csdK2* (B) loci.

A, B. Upper diagrams, transcription direction is indicated by the orientation of arrows, kinked arrows indicate transcription start sites as mapped in [24]. Coordinates indicate bp relative to the transcription start site of *csdK1* and *csdK2,* respectively. The lower diagrams show data from RNAseq as base-by-base alignment coverage for total RNA isolated from cells growing in 1% CTT broth [24]. Positive and negative values indicate reads mapped to the forward and reverse strand, respectively. Reads assigned to a gene are colored according to the gene color code in the upper diagrams. Red triangles indicate the CdbA peak summits from a ChIP-seq analysis in which an active CdbA-FLAG protein was used as bait [11].

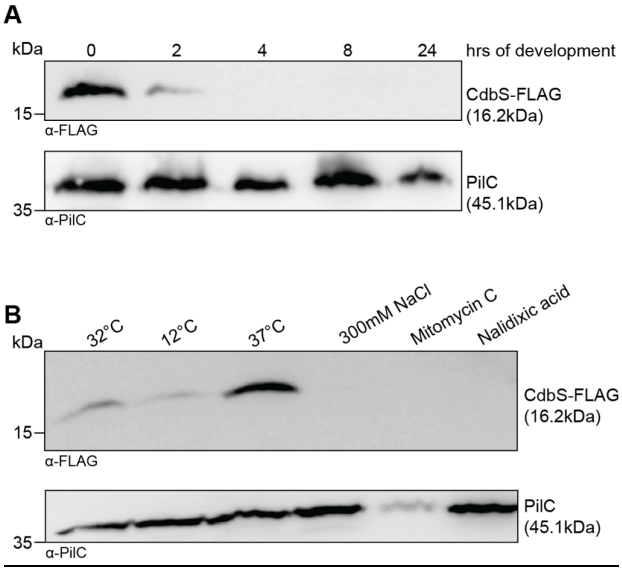

S11 Fig. Immunoblot analysis of CdbS-FLAG accumulation under different stress conditions. **A.** CdbS-FLAG accumulation decreases during development. Cells were developed under submerged conditions and harvested at the indicated time points. The same amount of protein was loaded per lane. PilC was used as a loading control. Similar results were obtained in two independent experiments. **B.** CdbS-FLAG accumulates at an increased level at 37°C. Cells were exposed to the indicated stresses for 18hrs and then harvested. The same amount of protein was loaded per lane. PilC was used as a loading control. Similar results were obtained in two biological replicates. CdbS-FLAG was synthesized from the native *cdbS* locus.

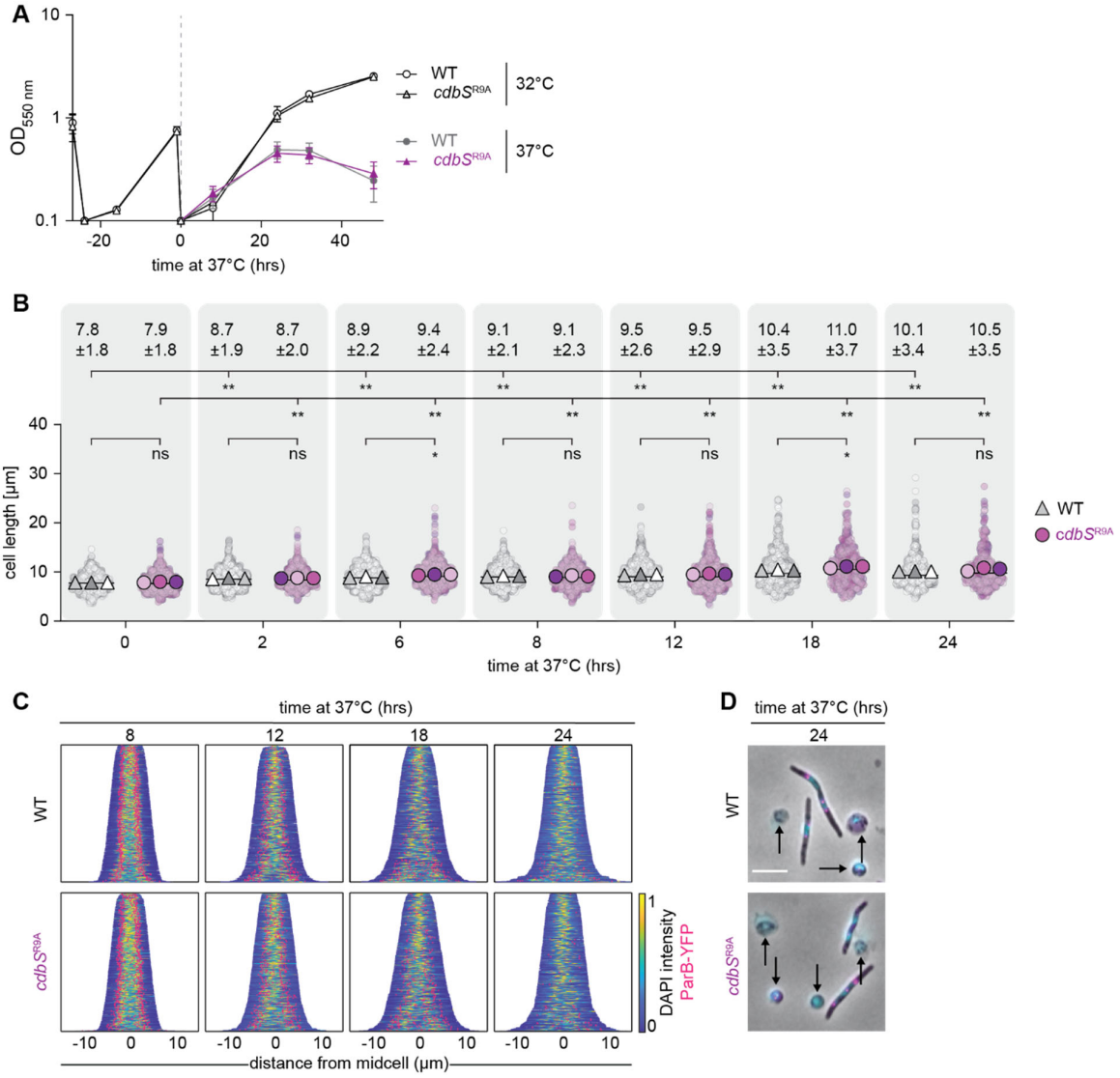

S12 Fig. CdbS accelerates cell death at 37°C independently of c-di-GMP binding.

A. Growth of strains of indicated genotypes. Cells were grown in 1% CTT broth in suspension culture at the indicated temperatures. Growth curves were generated from three biological replicates. All strains are *parB*$^{+}$/*parB-YFP* merodiploid. **B, C.** Cell length analyses (B) and chromosomes organization (C) in strains of the indicated genotypes during growth at 37°C. Cells were grown at 37°C for indicated periods. In B, cell length measurements are included from three independent experiments indicated in different colored triangles and the mean is based on all three experiments. Numbers above indicate cell length as mean ± STDEV calculated from all three experiments. *, *P*< 0.05, **, P< 0.01 and ns, not significant in 2way ANOVA multiple comparisons test. Only rod-shaped cells were included in the measurements. Total number of cells analyzed: 421-938. In C, only rod-shaped cells were included in the analysis and not cell that were undergoing lysis or had rounded up (See E) and cells are sorted according to length, DAPI signals are shown according to the intensity scale, and ParB-YFP signals in pink. N=400 cells for all strains. **D.** Microscopic analysis of cells of the indicated genotypes at 37°C for the indicated period. Cells were stained with DAPI (blue signal) and synthesizing ParB-YFP (pink signal). Arrows point to cells that have

lost their rod-shape and rounded up. Scale bar, 5 μm. A-D, both strains are *parB*$^{+}$/*parB-YFP* merodiploid.

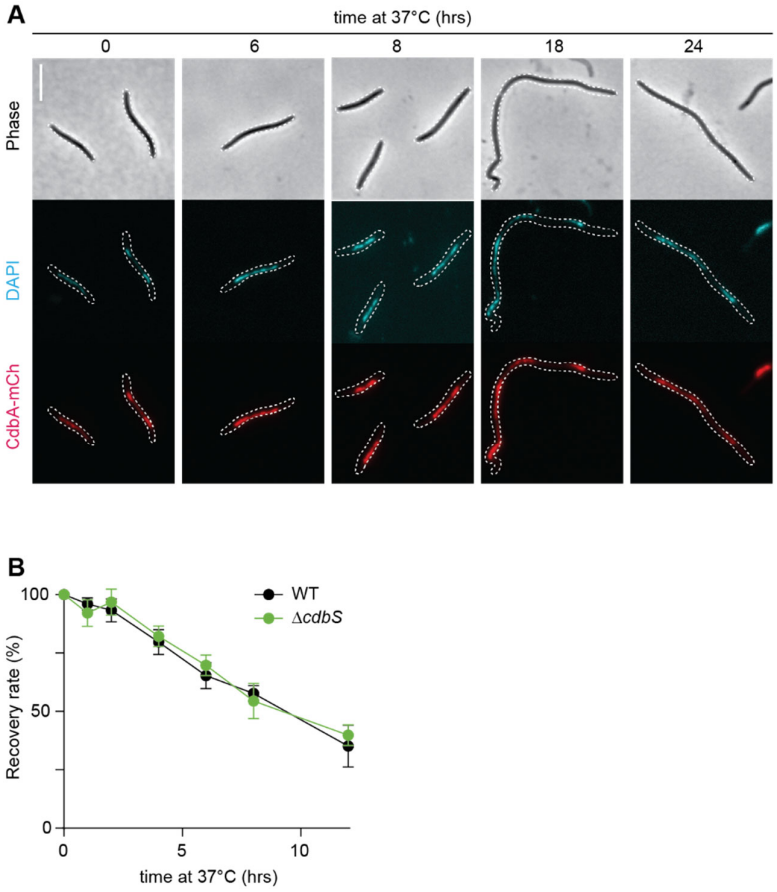

S13 Fig. Analysis of CdbA and CdbS at 37°C.

A. CdbA-mCh colocalizes with the nucleoid at 37°C. Cells of the indicated genotype were incubated at 37°C for the indicated periods. Phase contrast and fluorescence microscopy images of cells of the indicated genotype stained with DAPI and synthesizing CdbA-mCh. Scale bar, 5μm. CdbA-mCh was synthesized from the native *cdbA* locus. The strain is *parB*$^{+}$/*parB-YFP* merodiploid. **B.** CdbS does not provide a protective function at 37°C. Cells of the indicated genotypes were incubated at 37°C for the indicated periods and then plated at 32°C. Data represent the mean ± STDEV of three biological replicates normalized to the number of colony forming units at t=0hrs at 37°C (100%). In pairwise comparisons, no significant differences were observed in Student's t-test.

1399 **S1 Table.** Mutations identified by whole genome sequencing of suppressors of CdbA-mCh
1400 essentiality

Suppressor mutant	Gene locus	Mutation	Position of mutation	Amino acid change[1]
#2	*mxan_4328 (cdbS)*	C → T	60bp upstream of transcriptional start site	NA
	mxan_3823	G → T	261bp downstream of first nucleotide in start codon	T → T (silent)
#5	*mxan_4328 (cdbS)*	A → C	95bp downstream of first nucleotide in start codon	V32G
#8	*mxan_4328 (cdbS)*	T → C	67bp upstream of transcriptional start site	NA
#12	*mxan_4362 (cdbB)*	A → G	65 bp downstream of first nucleotide in start codon	Q22R
#14	*mxan_4328 (cdbS)*	G → A	226bp downstream of first nucleotide in start codon	Q76stop
#15	*mxan_4328 (cdbS)*	A → C	95bp downstream of first nucleotide in start codon	V32G
#18	*mxan_4328 (cdbS)*	T → C	67bp upstream of transcriptional start site	NA
#19	*mxan_4328 (cdbS)*	A → C	95bp downstream of first nucleotide in start codon	V32G
	mxan_3618	A → C	640bp downstream of first nucleotide in start codon	A → A (silent)

1401

1402 [1] NA, not applicable

1403

1404 **S2 Table.** *M. xanthus* strains used in this study.

Strain	Genotype	Reference
DK1622	WT	[52]
SA5691	Δ*cdbA*; *mxan18-19*::P_{van} *cdbA-mCh*; *parB*$^{+}$/*attB*::P_{nat} *parB-YFP*	[11]
SA5693	*parB*$^{+}$/*attB*::P_{nat} *parB-YFP*	[11]
SA8813	*cdbA*::*cdbA-FLAG*	[11]
SA11494	*attB*::P_{pilA} *gfp-FLAG*	This study
SA10209	Δ*cdbA*; *mxan18-19*::P_{van} *cdbA-mCh*; *cdbS*::*cdbS-FLAG; parB*$^{+}$/*attB*::P_{nat} *parB-YFP*	This study
SA10217	*cdbS*::*cdbS-FLAG; parB*$^{+}$/*attB*::P_{nat} *parB-YFP*	This study
SA10220	Δ*cdbS; parB*$^{+}$/*attB*::P_{nat} *parB-YFP*	This study
SA10225	Δ*cdbS*; *mxan18-19*::P_{van} *cdbS-FLAG*; *parB*$^{+}$/*attB*::P_{nat} *parB-YFP*	This study
SA10226	Δ*cdbS*; *mxan18-19*::P_{van} *cdbS*^{R9A}*-FLAG*; *parB*$^{+}$/*attB*::P_{nat} *parB-YFP*	This study
SA10249	*cdbS*::*cdbS-FLAG*; Δ*csdK1; parB*$^{+}$/*attB*::P_{nat} *parB-YFP*	This study
SA10251	*cdbS*::*cdbS-FLAG*; Δ*csdK2; parB*$^{+}$/*attB*::P_{nat} *parB-YFP*	This study
SA10260	*cdbA*::*cdbA-mCh; parB*$^{+}$/*attB*::P_{nat} *parB-YFP*	This study
SA10262	Δ*cdbA*; *mxan18-19*::P_{van} *cdbA-mCh*; *cdbS*::*cdbS-FLAG;* Δ*csdK1; parB*$^{+}$/*attB*::P_{nat} *parB-YFP*	This study
SA10264	Δ*cdbA*; *mxan18-19*::P_{van} *cdbA-mCh*; *cdbS*::*cdbS-FLAG;* Δ*csdK2; parB*$^{+}$/*attB*::P_{nat} *parB-YFP*	This study
SA10267	*cdbS*::*cdbS-FLAG*; Δ*csdK1*; Δ*csdK2; parB*$^{+}$/*attB*::P_{nat} *parB-YFP*	This study
SA10270	Δ*cdbA*; *mxan18-19*::P_{van} *cdbA-mCh*; *cdbS*::*cdbS-FLAG;* Δ*grpS; parB*$^{+}$/*attB*::P_{nat} *parB-YFP*	This study
SA10273	Δ*cdbA*; *mxan18-19*::P_{van} *cdbA-mCh*; *cdbS*::*cdbS-FLAG;* Δ*hsp20_1; parB*$^{+}$/*attB*::P_{nat} *parB-YFP*	This study
SA10274	*cdbA*::*cdbA-mCh; cdbS*::*cdbS-FLAG; parB*$^{+}$/*attB*::P_{nat} *parB-YFP*	This study
SA10275	*cdbA*::*cdbA-mCh;* Δ*cdbS*; *mxan18-19*::P_{van} *cdbS-FLAG*; *parB*$^{+}$/*attB*::P_{nat} *parB-YFP*	This study
SA10277	Δ*cdbA*; *mxan18-19*::P_{van} *cdbA-mCh*; *cdbS*::*cdbS-FLAG;* Δ*csdK1;* Δ*csdK2; parB*$^{+}$/*attB*::P_{nat} *parB-YFP*	This study
SA10288	*csdK1*::*csdK1-mV*	This study
SA10289	*csdK2*::*csdK2-HA*	This study
SA12204	Δ*cdbA*; *mxan18-19*::P_{van} *cdbA-mCh*; *csdK1*::*csdK1-mV*	This study
SA12205	Δ*cdbA*; *mxan18-19*::P_{van} *cdbA-mCh*; *csdK2*::*csdK2-HA*	This study
SA12206	Δ*cdbA*; *mxan18-19*::P_{van} *cdbA-mCh*; Δ*cdbS; parB*$^{+}$/*attB*::P_{nat} *parB-YFP*	This study
SA12209	Δ*cdbA*; *mxan18-19*::P_{van} *cdbA-mCh*; *cdbS*::*cdbS-FLAG;* Δ*mxan_0750; parB*$^{+}$/*attB*::P_{nat} *parB-YFP*	This study
SA12222	Δ*cdbA*; *mxan18-19*::P_{van} *cdbA-mCh*; Δ*cdbS; attB*::P_{nat} *cdbS-FLAG*::P_{nat} *parB-yfp*	This study

SA12238	*dnaB*^{A116V}; *parB*$^{+}$*/attB::P*$_{nat}$ *parB-YFP*	[36] & this study

1405

1406

1407 **S3 Table.** Plasmids used in this study.

Plasmid	Description	Reference
pBJ114	*galK*, Kan^R	[73]
pET28a(+)	Expression vector, Kan^R	Novagen® Merck (Darmstadt)
pMR3691	*mxan18-19* site integration, *vanR*-P_{van}, Tet^R	[30]
pSW105	Mx8 *attB* site integration, P_{pilA}, Kan^R	[74]
pSWU19	Mx8 *attB* site integration, Kan^R	[75]
pSWU30	Mx8 *attB* site integration, Tet^R	[76]
pUT18	BACTH plasmid, *cyaAT18* N-terminal fusion, Amp^R	Euromedex (Souffelweyersheim, France)
pUT18C	BACTH plasmid, *cyaAT18* C-terminal fusion, Amp^R	
pKNT25	BACTH plasmid, *cyaAT25* N-terminal fusion, Kan^R	
pKT25	BACTH plasmid, *cyaAT25* N-terminal fusion, Kan^R	
pDJS94	pBJ114; Δ*csdK2*, Kan^R	[23]
pDJS151	pSWU19; P_{nat} *parB-YFP*, Kan^R	[11]
pMAT219	pSW105; *gfp-FLAG*, Kan^R	[77]
pSK42	pBJ114; Δ*csdK1*, Kan^R	[23]
pMS007	pET28a(+); His_6-*cdbS*, Kan^R	This study
pMS008	pET28a(+); His_6-*cdbS*^{R9A}, Kan^R	This study
pMS018	pBJ114; *cdbS-FLAG*, Kan^R	This study
pMS024	pMR3691; P_{van} *cdbS-FLAG*, Tet^R	This study
pMS026	pMR3691; P_{van} *cdbS*^{R9A}*-FLAG*, Tet^R	This study
pMS054	pBJ114; *cdbA-mCh*, Kan^R	This study
pMS055	pBJ114; Δ*dnaJ1*, Kan^R	This study
pMS056	pBJ114; Δ*grpS*, Kan^R	This study
pMS057	pBJ114; Δ*hsp20_1*, Kan^R	This study
pMS088	pBJ114; *csdK1-mV*, Kan^R	This study
pMS089	pBJ114; *csdK2-HA*, Kan^R	This study
pMS102	pSWU19; P_{nat} *parB-YFP*; P_{nat} *cdbS-FLAG*; Kan^R	This study
pKNT25-CdbS	pKNT25; *cdbS*, Kan^R	This study
pKT25-CdbS	pKT25; *cdbS*, Kan^R	This study
pUT18-CdbS	pUT18; *cdbS*, Amp^R	This study
pUT18C-CdbS	pUT18C; *cdbS*, Amp^R	This study
pKT25-CsdK1	pKT25; *csdK1*, Kan^R	This study
pUT18C-CsdK1	pUT18C; *csdK1*, Amp^R	This study
pKT25-CsdK2	pKT25; *csdK2*, Kan^R	This study
pUT18C-CsdK2	pUT18C; *csdK2*, Amp^R	This study
pKNT25-DnaB	pKNT25; *dnaB*, Kan^R	This study
pKT25-DnaB	pKT25; *dnaB*, Kan^R	This study
pUT18-DnaB	pUT18; *dnaB*, Amp^R	This study
pUT18C-DnaB	pUT18C; *dnaB*, Amp^R	This study
pKT25-CdbS^{R9A}	pKT25; *cdbS*^{R9A}, Kan^R	This study
pUT18C-CdbS^{R9A}	pUT18C; *cdbS*^{R9A}, Amp^R	This study
pKT25-CsdK2^{R38A}	pKT25; *csdK2*^{R38A}, Kan^R	This study
pUT18C-CsdK2^{R38A}	pUT18C; *csdK2*^{R38A}, Amp^R	This study
pKT25-CsdK2$^{1-435}$	pKT25; *csdK2*$^{1-435}$, Kan^R	This study

pUT18C-CsdK2$^{1-435}$	pUT18C; *csdK2* $^{1-435}$, Amp^{R}	This study
pKT25-CsdK2$^{1-435_R38A}$	pKT25; *csdK2* $^{1-435\_R38A}$, Kan^{R}	This study
pUT18C-CsdK2$^{1-435_R38A}$	pUT18C; *csdK2* $^{1-435\_R38A}$, Amp^{R}	This study
pKT25-CsdK2$^{298-1146}$	pKT25; *csdK2* $^{298-1146}$, Kan^{R}	This study
pUT18C-CsdK2$^{298-1146}$	pUT18C; *csdK2* $^{298-1146}$, Amp^{R}	This study

1408

1409

1410 **S4 Table.** Primers used in this study.

Primer name	Sequence (5'→3')
CdbS_E	GAGGCGCTCCAGTACATCGC
CdbS_F	CCGCCAACATCCTGTCGCAG
CdbS_G	ACCTCCGTTTCGACAAGGTC
CdbS_H	GTCGTCCTGCGTCTCATAGG
CdbA_E	GAAGCCGGAGTCGCTC
CdbA_F	GCCAGCCGAAAGGCTC
CdbA_G	CAGTCGCTGTACTTCCCC
CdbA_H	CTCGTCGCCAGTCACA
CsdK1_E	CACCTTCACCGCGTCCACGC
CsdK1_F	GGGCTCCGCGCCGCAGAA
CsdK1_G	TTCCCCCGGTTCCTCCCAAT
CsdK1_H	ATGGAGGGCACCGTGTTGTG
CsdK2_E	TGTGAACCACGCCAGGCTGCC
CsdK2_F	GCAGTGCCCGTCCTCGCGCTT
CsdK2_G	AAGGGCTTCCCCAAGTGCGCC
CsdK2_H	TTGAGCTCGCGGTTGAGACCG
4328 fw_NdeI	ATGCATATGATGTTTGAGCGTCCTCACGA
oMS002	ATGTCTAGAATGTTTGAGCGTCCTCACGAGCGCGCGTCCCACCTC
oMS004	GTTAAGCTTTCAGTGCATCACCCGCTCGCGGTCG
oMS013	CTGCCCGCCGCGCTGCCCGCGCTGCCGTGCATCACCCGCTCGCGGTC
oMS024	GATAAGCTTGGTTCAGCCCGGAATCGTGCC
oMS025	GCGGGCAGCGCGGCGGGCAGCGGCGAGTTCGACTACAAGGACGACGACGACAAGTGACGTCCGCCCGGGGCCCGTGAGG
oMS026	CAGTGAATTCGAGCTCATCCCGGACATC
oMS029	GCGGGCAGCGCGGCGGGCAGCGGCGAGTTCATGAGCAAAGGAGAAGAACTT
oMS041	GAGGAATTCTCACTTGTCGTCGTCGTCCTTG
oMS068	CCTTCTAGAGAGGCGTGTCATCGTCACCCG
oMS068	CCTTCTAGAGAGGCGTGTCATCGTCACCCG
oMS069	GCCTGCATGCTCACTTGTACAGCTCGTCCA
oMS070	TACGAATTCGAGCTCGGTACCGGGGATCCTCTAGAGTCGACCTGCAGGCATGCAAGCTTGGCAC
oMS071	GTGCCAAGCTTGCATGCCTGCAGGTCGACTCTAGAGGATCCCCGGTACCGAGCTCGAATTCGTA
oMS082	GCCAAGCTTCGGACCGCGGTGGAATGGAG
oMS083	TCTTCTAGAGGATCCCTCCTCCCGAGGGTCCTGGC
oMS084	GAGGGATCCTCTAGAAGATCTGCTAGCGGCAGCGCGGCGGGCAGCGGCATGGTGAGCAAGGGCGAGGAG
oMS085	GTCCGTCGTAGCCATCCGTCGTTACTTGTACAGCTCGTCCATG
oMS086	CATGGACGAGCTGTACAAGTAACGACGGATGGCTACGACGGAC
oMS087	AGTGAATTCGAGACGGCTATGGCACGGCGC
oMS092	GCCAAGCTTATCGGTTATACGGACATCAAG
oMS093	CTTCACCTTGGCGATGTCGCGTTTCTGACCCGCCGC
oMS094	ATCGCCAAGGTGAAGGAGCTG
oMS095	AGTGAATTCGAAGAAGAGGACGCCGGCCTG
oMS096	CAACCCTGCGGACAGGTTCAG
oMS097	GGCGTCATCCGCCCGCGAATG
oMS098	GAAATCTGTCTCCGCGCAGGA
oMS099	CTCCGCGAACTTCTCCAGCAG
oMS100	GCCAAGCTTGAGCGCCTCCTCAAGGAAGTG
oMS101	GGAAGAGTTCTCGGACTTGTCGTTCGAGCCGGCCAC

oMS102	GTCCGAGAACTCTTCCGGGGGGAGTCAG
oMS103	CAGTGAATTCGCAGGACACTGAGCCCGGCGA
oMS104	GATGACTGCCCCATGGAGGAG
oMS105	AGCTCCAGGATGGAGATATCG
oMS106	CATTGACGCGGCGGTTCGCAG
oMS107	CTCGGTGTCGGTCGTGGCGGTG
oMS116	GCCAAGCTTATGATGCGCGACAGACGTCCG
oMS117	GACTTCGATGACGCGGGCGGAGTTGAACGGATTGCGAGTCT GCAT
oMS118	CGCGTCATCGAAGTCAAGGTC
oMS119	AGTGAATTCCCTGCGCACGTTCCTCATCAC
oMS120	GCACCAGCGTCTTGCCGTTGTC
oMS121	CAGCGGAATCATGCAGCAAGAG
oMS122	CGAGCTGACGCAGCCCATGTG
oMS123	GTCAGCGTCAGCACACCCTGC
oMS131	GACTCTAGAGATGTTTGAGCGTCCTCACGAG
oMS132	GCTCGGTACCTTGTGCATCACCCGCTCGCGGTC
oMS133	GACTCTAGAATTGACGGAATCGAATCAGGCG
oMS134	CTCGGTACCTTGGCTCTTCCGAACAACCCCTTG
oMS135	GACTCTAGAAGTGGTCTGCCCACCTGTCGAC
oMS136	ATTGAATTCTTCTTCCTGCCCAGCGCCTTCTT
oMS141	ATTGAATTCTTAGTTCTTCCTGCCCAGCGCCTTCTT
oMS154	GACTCTAGAGATGGAGAACGTCCACGAG
oMS155	CTCGGTACCAGCTCGCTCCGCGACCGGCTC
oMS177	GCCAAGCTTGACGAAGAGCTACACCCTG
oMS180	CAGTGAATTCCGCGAGTGAGAGGATGC
oMS182	GCCAAGCTTGTCAACGCGGACGAAGCC
oMS183	TGGGACGTCGTATGGGTACTTCCTGCCCAGCGCCT
oMS184	TACCCATACGACGTCCCAGACTACGCTTGATGGTCACATCCT CAATTCGAAAAG
oMS185	CAGTGAATTCCGCTGGAGCACCGACAAC
oMS187	GATAAGCTTGTGGTGCCCATCGCGTC
oMS188	CCGCGCTGCCCGCGCTGCCCTCGCTCCGCGACCGGCTC
oMS189	CAGCCCTCCGTGTTCGCG
oMS190	GTAGAATTCCCACCACCAGTCGGTGC
oMS191	GCATCGGCAAGACGTCC
oMS192	CGGTGAAGTGCGGCATG
oMS193	GAACACGGAGGGCTGTTATTTGTAGAGCTCATC
oMS194	CGGGCAGCGCGGCGGGCAGCGGCGAGTTCATGGTGAGCAA GGGCGAG
oMS204	GATCAAGGCAGGGCCACCACGGACAGG
oMS205	CCTGTCCGTGGTGGCCCTGCCTTGATC
oMS206	GTAGAATTCGGGCTCACGTCCTCGGCCA
oMS207	GTATCTAGAAGACTACAAGGACGACGACGACAAGCTGGACA TCGATGAGCC
oMS208	GTAGAATTCCTATGGGCTCACGTCCTCGGCCAG
oMS211	CTGTTCGCATATGTCACTTGTACAGCTCGTCCA
oMS212	AAGTGACATATGCGAACAGAAAGTAATCGTATGCTCTGCGG GGTGAAGAC
oMS228	GAAAACGCGCACTGCGTG
oMS231	CCGCGCTGCCCGCGCTGCCGGCTCTTCCGAACAACCC
oMS232	CGCAGTGCGCGTTTTCACTTGTACAGCTCGTCCATG
cdbS qPCR fwd	CCGTTTCGACAAGGTCTTCA
cdbS qPCR rev	GGACCTCCACGAACATGC
csdK1_ter 1 qPCR fwd	TTCCACTATGAGATCGCGGC
csdK1_ter 1 qPCR rev	CTGATGGCCCAACTGGTTCT

csdK2 qPCR fwd	GGGGATCGAGGGGTCAAAAC
csdK2 qPCR rev	GCTTCAGCTTCA
rpsS qPCR fwd	GTTCGATCAAGAAGGGTCCGT
rpsS qPCR rev	GACGAACACCGGGATGAACT
ori 1/dnaA fwd	AACCTCATCTGGGAGCGAGA
ori 1/dnaA rev	TTGCCGAGGAACTGGATGTC
ori 2/7483 fwd	TGCCCACCATCAATCCATCC
ori 2/7483 rev	TGAGTTCCTGACGCTTGGTG

1411